Small non-coding RNA CjNC110 influences motility, autoagglutination, AI-2 localization, and chicken colonization in *Campylobacter jejuni*

Amanda J. Kreuder[1,2#], Brandon Ruddell[2], Kathy Mou[2*], Alan Hassall[1,2], Qijing Zhang[2], Paul J. Plummer[1,2]

[1] Department of Veterinary Diagnostic and Production Animal Medicine, College of Veterinary Medicine, Iowa State University, Ames, IA, United States

[2] Department of Veterinary Microbiology and Preventive Medicine, College of Veterinary Medicine, Iowa State University, Ames, IA, United States

#Address correspondence to Amanda J. Kreuder, akreuder@iastate.edu

* Current Address: United States Department of Agriculture, Agricultural Research Service, National Animal Disease Center, Ames, IA United States; and Oak Ridge Institute for Science and Education, Oak Ridge, TN, United States

Amanda J. Kreuder and Brandon Ruddell contributed equally to this work. Author order was determined on the basis of seniority.

Abstract

Small non-coding RNAs are involved in many important physiological functions in pathogenic microorganisms. Previous studies have identified the presence of non-coding RNAs in the major zoonotic pathogen *Campylobacter jejuni*, however, few have been functionally characterized to date. CjNC110 is a conserved ncRNA in *C. jejuni*, located downstream of the *luxS* gene which is responsible for the production of the quorum-sensing molecule autoinducer-2 (AI-2). In this study, we utilized strand specific high-throughput RNAseq to identify potential targets or interactive partners of CjNC110 in a sheep abortion clone of *C. jejuni*. This data was utilized to focus further phenotypic evaluation of the role of CjNC110 in growth, motility, autoagglutination, quorum sensing, and chicken colonization in *C. jejuni*. Inactivation of the CjNC110 ncRNA led to a statistically significant decrease in autoagglutination ability as well as increased motility when compared to wild-type. Extracellular AI-2 detection was decreased in ΔCjNC110, however, intracellular AI-2 accumulation was significantly increased with a concurrent increase in LuxS expression, suggesting a key role of CjNC110 in modulating the transport of AI-2. Notably, ΔCjNC110 also showed a significant defect in the ability to colonize chickens. Complementation of CjNC110 restored all phenotypic changes back to wild-type levels. The collective results of the phenotypic and transcriptomic changes observed in our data provide valuable insights into the pathobiology of *C. jejuni* sheep abortion clone and strongly suggest that CjNC110 plays an important role in regulation of energy taxis, flagellar glycosylation, cellular communication via quorum sensing, and chicken colonization in this important zoonotic pathogen.

Introduction

Campylobacter jejuni is a major foodborne and zoonotic pathogen that causes enteritis in humans [1]. A sheep abortion (SA) clone, with IA3902 as the prototype strain, has recently emerged as the predominant cause of ovine abortion [2] and as an important pathogen in foodborne outbreaks of human gastroenteritis [3] in the United States. *C. jejuni* clone SA is also widely distributed in the cattle population in the U.S. [4]. The genome of IA3902 is quite syntenic with that of *C. jejuni* type-strain NCTC 11168 [5] although it is much more virulent than NCTC 11168 in inducing systemic infection and abortion in animals. Despite its hypervirulence, *C. jejuni* IA3902 does not harbor any virulence factors known to be associated with abortion in *C. fetus* subsp. *fetus* [6, 7]. Previously, the *luxS* gene, which mediates autoinducer-2 (AI-2) production, and the genes coding capsular polysaccharide have been identified as critical for intestinal colonization and/or translocation across gut epithelium into the bloodstream [8] [9]. Point mutations in the major outer membrane protein encoded by *porA* have also been shown to be sufficient to cause the abortion phenotype when compared to the syntenic non-abortive strain NCTC 11168 [10]. The fact that relatively mild changes in genomic sequences have led to significantly enhanced ability to cause disease by *C. jejuni* IA3902, as described above, suggests that even slight differences in sequence variations or gene regulation may have a major impact on virulence variation among differing strains of *C. jejuni*.

C. jejuni has only three known sigma factors that regulate gene transcription: σ^{70} (encoded by *rpoD*), σ^{54} (encoded by *rpoN*) and σ^{28} (encoded by *fliA*) [11]. Besides control at the transcriptional level, regulation of gene expression can also occur by post-transcriptional

modulation of mRNA translation, stability and processing, for which small non-coding RNAs are the primary players [12-14]. Non-coding RNAs (ncRNAs) can be rapidly produced and serve to regulate multiple different targets within a cell in a variety of ways to coordinate rapid responses to changing environments. Thus, regulation of cellular processes by ncRNAs can provide several advantages to the bacteria when compared to the traditional model of protein-mediated regulation [15].

Prior to completion of the transcriptional start site map via high throughput RNA sequencing (RNAseq) of *H. pylori* [16], the ε-proteobacteria were thought not to be capable of using small and antisense RNA as a regulatory mechanism, partly due to a lack of the small RNA chaperone protein Hfq [17]. Indeed, attempts using computational approaches to identify ncRNAs in *Campylobacter* failed to yield any potential candidates, with only 3 potential loci being identified in *Helicobacter* [18]. Recently, clear evidence that *C. jejuni* also harbors these important regulators has been published, revealing the existence and expression of a wealth of ncRNAs present in strains such as NCTC 11168, 81-176, 81116, RM1221 and IA3902 [19-24]. Dugar *et al.* [21], when comparing the transcriptomes of 4 different *C. jejuni* isolates, observed a large variation in transcriptional start sites as well as expression patterns of both mRNA and ncRNA between strains. This suggests that variations in the existence and expression of ncRNAs even among closely related strains may play a role in differentiating virulence. Despite these advances, identification of the functions of ncRNAs in *Campylobacter* has been slow to follow, with most lacking functionally characterization.

The first report attempting to elucidate the role of two previously identified non-coding RNAs in *C. jejuni* suggests these ncRNAs may play a role in flagellar biosynthesis; however, the authors were unable to demonstrate phenotypic changes following inactivation of either non-coding RNA [25]. A later paper, however, did establish the role of an RNA antitoxin (*cjrA*) as the first noncoding antisense small RNA functionally characterized in *Campylobacter* to date [26]. Beyond simply establishing the existence of non-coding RNA transcripts in *Campylobacter*, there is critical need to continue to determine the physiological functions of these potential regulators in this important zoonotic pathogen.

Our previous work has demonstrated the *in vivo* and *in vitro* expression of numerous ncRNAs in *C. jejuni* IA3902 [24], including several that are conserved in other strains of *Campylobacter* [21]. One of the expressed ncRNAs identified in our study, the conserved small RNA CjNC110, is located in the intergenic region immediately downstream of the *luxS* gene. This ncRNA was of particular interest to our group as previous work in our lab has already highlighted the importance of the *luxS* gene in the virulence of *C. jejuni* [8]. In *Campylobacter*, the *luxS* gene is known to serve two important functions, production of the quorum sensing molecule autoinducer-2 (AI-2) and conversion of *S*-ribosylhomocysteine to homocysteine in the active methyl cycle (AMC) [27]. Of particular note, following the identification of CjNC110, it has also been suggested that different methods of generation of the *luxS* mutation may have led to polar effects on this downstream ncRNA that may help explain observed differences in phenotypes and gene expression between studies of *luxS* mutants in *Campylobacter* [28].

Based on these observations, in this study we chose to focus on elucidating the role of CjNC110 in the pathobiology of *C. jejuni* IA3902. Specifically, we investigated the effect of mutagenesis of either CjNC110 or *luxS* as well as combined mutation of both genes on the transcriptional landscape during exponential and stationary stages of growth of *C. jejuni* IA3902 using high-throughput RNA sequencing (RNAseq). Using RNAseq, we successfully demonstrated differences in the transcriptional landscape between our mutant constructs and

IA3902 wild-type. Based on the RNAseq data, we then utilized several phenotypic models to further demonstrate that inactivation of CjNC110 affects motility, autoagglutination activity, autoinducer-2 (AI-2) activity and chicken colonization. The work presented here provides compelling evidence that expression of the ncRNA CjNC110 is important for the pathobiology of *C. jejuni* IA3902.

Materials and methods

Ethics Statement

All studies involving animals were approved by the Iowa State University Institutional Animal Care and Use Committee (IACUC) prior to initiation (1-18-8675-G) and followed all appropriate animal care guidelines as set forth in the "Public Health Service Policy on Humane Care and Use of Laboratory Animals" developed by the U.S. Department of Health and Human Services, National Institutes of Health Office of Laboratory Animal Welfare. Humane euthanasia was performed using carbon dioxide asphyxiation as recommended by the American Veterinary Medical Association "Guidelines for the Human Euthanasia of Animals."

Bacterial strains, plasmids, primers and culture conditions

C. jejuni IA3902 was initially isolated from an outbreak of sheep abortion in Iowa during 2006 and has been utilized by our laboratory as the prototypical isolate of clone SA [2]. W7 is a highly motile variant of the commonly utilized laboratory strain *C. jejuni* NCTC 11168 [8]. *C. jejuni* strains and their isogenic mutants were routinely grown in Mueller-Hinton (MH) broth or agar plates (Becton-Dickinson, Franklin Lakes, NJ) at 42°C under microaerophilic conditions (5% O_2, 10% CO_2, 85% N_2). For the mutant strains containing a chloramphenicol resistance cassette, 5 μg/mL chloramphenicol was added to either the broth or agar plates when appropriate. For strains containing a kanamycin resistance cassette, 30 μg/mL kanamycin was added to either the broth or agar plates when appropriate.

For genetic manipulations, *Escherichia coli* competent cells were grown at 37°C on Luria-Bertani (LB) agar plates or broth (Becton-Dickinson, Franklin Lakes, NJ) with shaking at 125 rpm. When appropriate, 50 μg/mL kanamycin, 20 μg/mL chloramphenicol or 100 μg/mL ampicillin was added to the broth or agar plates for selection of colonies. *Vibrio harveyi* strains were grown in autoinducer broth (AB) at 30°C with shaking at 175 rpm as described previously [29].

All strains used in this study are described in **Table 1**, with all relevant plasmids listed in **Table A in S1 Appendix** and primer sequences and LNA probe sequence in **Table B in S1 Appendix**. All strains were maintained in 20% glycerol stocks at -80°C and passaged from those stocks as needed for experimental procedures.

Table 1. Bacterial strains utilized in this study.

Strain	Description	Source or Reference
Campylobacter jejuni		
W7	Wild-type motile variant of NCTC 11168	[8]
W7 ΔCjNC110	W7 ΔCjNC110::Cm^R	This study
Sheep Abortion (SA) IA3902	Wild-type *C. jejuni*	[2]
IA3902 ΔCjNC110	IA3902 ΔCjNC110::Cm^R	This study
IA3902 ΔluxS	IA3902 ΔluxS::Kan^R	[30]
IA3902 ΔCjNC110ΔluxS	IA3902 ΔCjNC110::Cm^R ΔluxS::Kan^R	This study
IA3902 ΔCjNC110c	IA3902 ΔCjNC110::Cm^R CjNC110::Kan^R	This study
Escherichia coli		
DH5α	*fhuA2* Δ(*argF-lacZ*)U169 *phoA gln*V44 Φ80 Δ(*lacZ*)M15 *gyrA*96 *recA1 relA1 endA1 thi-1 hsdR*17	New England Biolabs, Ipswich, MA
Vibrio harveyi		
BB152	AI-1-/AI-2+; luxM::Tn5	[29]
BB170	AI-2 reporter strain; luxN::Tn5	[31]

Kan^R = kanamycin resistance cassette

Cm^R = chloramphenicol resistance cassette

Creation of *C. jejuni* ΔCjNC110 and ΔCjNC110ΔluxS mutants in IA3902

An isogenic CjNC110 mutant of *C. jejuni* IA3902 was constructed via deletional mutagenesis utilizing a combination of synthetic double-stranded DNA (dsDNA) fragments and traditional cloning methods. Based on previously published data depicting the proposed transcriptional start site for CjNC110 [21], the coding region of CjNC110 in IA3902 and the prototypical *C. jejuni* strain 11168 were first confirmed to be identical. Then, a 200 bp section of the IA3902 genome starting 20 bp upstream and including the entire 137 nt transcript of the CjNC110 sequence as predicted in Dugar *et al.* [21] was replaced with 820 bp of the promoter and coding sequence of the chloramphenicol acetyltransferase (*cat*) gene of *Campylobacter coli* plasmid C-589 [32]. Synthetic dsDNA including approximately 500 bp upstream and 500 bp downstream of the region replaced with the *cat* cassette was then synthesized in 4 fragments of 500 bp each with overlapping homologous ends (Integrated DNA Technologies, Coralville, IA). The Gibson Assembly method was then utilized to assemble the synthetic dsDNA fragments [33] using the Gibson Assembly Master Mix (New England Biolabs, Ipswich, MA). Following assembly, primers (CJnc110F2 and CJnc110R2) were designed to amplify a 1785 bp product of the assembled dsDNA; PCR amplification was achieved using TaKaRa Ex Taq DNA Polymerase (ClonTech, Mountain View, CA). This amplified PCR product was then cloned into the pGEM-T Easy Vector using T4 ligase (Promega, Madison, WI), resulting in the construction of pCjNC110::cat which was then transformed into chemically competent *E. coli* DH5α (New England Biolabs, Ipswich, MA). Transformants were then selected on LB agar plates containing

chloramphenicol (20 μg/ml), ampicillin (100 μg/ml), and ChromoMax IPTG/X-Gal Solution (Fisher Scientific, Pittsburgh, PA). pCjNC110::cat was purified from the transformed *E. coli* using the QIAprep Miniprep kit (QIAGEN, Germantown, MD) and confirmed by PCR to contain the construct again using the CJNC110F2 and CJNC110R2 primers.

The pCjNC110::cat plasmid DNA was then introduced to *C. jejuni* W7 as a suicide vector and the deletion transferred into the genome of *C. jejuni* W7 via homologous recombination. Transformants were selected on MH agar plates containing chloramphenicol (5 μg/ml) and deletional mutagenesis was again confirmed via PCR analysis and Sanger sequencing to create *C. jejuni* W7ΔCjNC110. Following confirmation, natural transformation was used to move the gene deletion into *C. jejuni* IA3902 as previously described [34] to create *C. jejuni* IA3902ΔCjNC110. Natural transformation was again used to move the CjNC110 gene deletion into the previously created *luxS* insertional mutant *C. jejuni* IA3902ΔluxS [8] to create the double knockout mutant *C. jejuni* IA3902ΔCjNC110ΔluxS. Transformants were selected on MH agar plates containing chloramphenicol (5 μg/mL) and kanamycin (30 μg/mL) and confirmed via PCR analysis and Sanger sequencing of the CjNC110 region along with the entire upstream (*luxS*) and downstream (CjSA_1137) genes using primers Cj1198F1 and Cj1199R3. All colonies were screened for presence/absence of motility as described below, and only colonies with verified motility were used for future studies. Expression of CjNC110 in wild-type and elimination of expression in the ΔCjNC110 mutant was confirmed via northern blot analysis using an LNA custom designed probe (QIAGEN) and 15μg of total RNA as previously described [35].

Creation of *C. jejuni* ΔCjNC110 complement in IA3902

Complementation of ΔCjNC110 was achieved via insertion of the coding region into the intergenic region of the 16S and 23S rRNA operon (*rrs-rrl*) of IA3902ΔCjNC110 via homologous recombination using plasmid pRRK. A copy of the CjNC110 gene including 190bp upstream of the transcription initiation location (total of 570bp) was cloned into an *XbaI* site of pRRK located upstream of the kanamycin resistance determinant to create pCjNC110c as previously described in our lab [36] with some modifications of the original protocol [37]. Briefly, the CjNC110 gene and flanking regions of IA3902 were amplified using forward and reverse primers designed with an *XBaI* restriction enzyme site (CjNC110cF1 and CjNC110cR1). Following PCR amplification with TaKaRa Ex Taq DNA Polymerase (ClonTech, Mountain View, CA), the PCR product and pRRK plasmid were digested with the *XBaI* restriction endonuclease (New England Biolabs, Ipswich, MA). The digested plasmid was then incubated twice with Antarctic Phosphatase (New England Biolabs, Ipswich, MA) to prevent self-ligation of cut plasmid. Following ligation and transformation, transformants were selected on LB agar plates containing chloramphenicol (20 μg/ml) and kanamycin (50 μg/ml kanamycin) yielding a plasmid containing the construct pRRK::CjNC110 in *E. coli* DH5α. Following PCR confirmation and Sanger sequencing to confirm preservation of correct gene sequence, the plasmid was then utilized as a suicide vector and the gene was inserted into the intergenic region of the 23S rRNA operon (*rrs-rrl*) of IA3902ΔCjNC110 via homologous recombination to generate IA3902ΔCjNC110c transformants. The transformants were selected on MH agar plates containing chloramphenicol (5 μg/ml) and kanamycin (30 μg/ml) and confirmed via PCR analysis and Sanger sequencing to contain both the expected ΔCjNC110 deletional mutation and ΔCjNC110c insertion, validating successful genetic complementation. All positive colonies

were screened for presence/absence of motility as described below and a motile complement was selected to create IA3902ΔCjNC110c.

Growth curves

Two separate growth curves were completed in triplicate utilizing the same method as described below with the only variation being the addition of the complement strain ΔCjNC110c to the second growth curve. To begin the growth curve, the A_{600} of overnight cultures were adjusted to 0.5 using sterile MH broth on a Genesys 10S VIS spectrophotometer (Thermo Scientific™, Waltham, MA). Cultures were then diluted 1:10 for a final targeted starting A_{600} of 0.05 in 90 mL sterile MH broth and placed in a sterile 250 mL Erlenmeyer glass flask. Cultures were incubated at 42°C under microaerophilic conditions with shaking at 125 rpm for 30 hours with removal of samples from the flasks at designated time points [3, 6, 9, 12, 24, 27 (2nd growth curve only) and 30 hours]. For the first growth curve (which included the following strains: IA3902 wild-type, ΔCjNC110, ΔluxS and ΔCjNC110ΔluxS), samples were processed as described below for RNA isolation as well as assessed for A_{600} and actual colony counts using the drop-plate method as previously described [38]. For the second growth curve (which included ΔCjNC110c in addition to the four previous strains), samples were collected and processed for A_{600} and as described below for assessment of AI-2 levels via the bioluminescence assay. The A_{600} over time were statistically analyzed for the two independent growth curves, using a two-way ANOVA with repeated measures and Dunnett's multiple comparison test (GraphPad Prism).

Total RNA extraction

Broth culture samples processed for total RNA extraction were either centrifuged at 8000 x *g* for 2 minutes (for sequencing and qRT-PCR) or 10,000 x *g* for 4 minutes (Northern blot) at 4°C immediately following collection. Following pelleting of the cells, the supernatant was decanted and 1 mL QIAzol Lysis Reagent (QIAGEN) was added to resuspend the cell pellet and protect the RNA. QIAzol-protected cultures were then stored at -80°C for up to two months prior to proceeding with total RNA isolation. Total RNA isolation was performed using the miRNeasy Mini Kit (QIAGEN) followed by purification using the RNeasy MinElute Cleanup kit (QIAGEN) as previously described [24]. RNA quality was measured using the Agilent 2100 Bioanalyzer RNA 6000 Nano kit (Agilent Technologies, Santa Clara, CA) and all RNA samples utilized for downstream RNAseq library preparation had an RNA integrity number (RIN) of >9.0, indicating high quality RNA. Verification of complete removal of any contaminating DNA was performed via PCR amplification of a portion of the CjSA_1356 gene, which is unique to *C. jejuni* IA3902, using primers SA1356F and SA1356R [39].

RNAseq library preparation and sequencing

The 3 hour (exponential phase) and 12 hour (stationary phase) timepoints were selected for RNAseq analysis based on assessment of $\log_{10}$ CFU/mL (**Fig A in S3 Appendix**). 2.5 µg of confirmed DNA-free total RNA was treated with Ribo-Zero rRNA Removal Kit for Bacteria according to the manufacturer's instructions (Illumina, San Diego, CA). Following rRNA removal, the ribosomal depleted total RNA was purified using the RNeasy MinElute Cleanup kit (QIAGEN) using the same modifications as described previously [24]. Following clean-up, the RNA quality, quantity, and rRNA removal efficiency was then analyzed via the Agilent 2100

Bioanalyzer RNA 6000 Pico kit (Agilent Technologies). Library preparation for sequencing on the Illumina HiSeq platform was completed using the TruSeq stranded mRNA HT library preparation kit (Illumina) with some modifications as described previously [24]. The pooled library was then submitted to the Iowa State University DNA Facility and sequenced on an Illumina HiSeq 2500 machine in high-output single read mode with 100 cycles.

Differential gene expression analysis of RNAseq data

Rockhopper (http://cs.wellesley.edu/~btjaden/Rockhopper/) was used to analyze the differences in gene expression between strains and timepoints; the standard settings of the program were utilized for analysis [40]. Following computational analysis via Rockhopper, a change in gene expression was deemed significant when the Q-value (false discovery rate) was below 5% and a >1.5 fold change in expression was observed. Visual assessment of read count data was performed using the Integrated Genome Viewer (IGV) (https://www.broadinstitute.org/igv/) [41, 42]. Assessment of function of the differentially expressed genes was performed using the Clusters of Orthologous Groups (COG) [43] as previously described in IA3902 [5]. Venn diagrams were used to depict overlap of genes differentially regulated in multiple mutant strains and were generated using BioVenn [44] (http://www.cmbi.ru.nl/cdd/biovenn/index.php). Kegg Pathways was used to perform metabolic pathway analysis [45] (http://www.genome.jp/kegg/pathway.html).

Northern Blot

For northern blot detection of CjNC110, bacterial cells from WT, ΔCjNC110, and ΔCjNC110c were grown to exponential phase of growth in MH broth and total RNA isolation performed as described above. The total RNA input was normalized to 15 µg using Qubit™ BR RNA Assay Kit (Invitrogen™, USA) for each respective strain. For northern blot detection**,** total RNA from bacterial cells (15 µg) and a pre-stained DynaMarker® RNA High Ladder (Diagnocine LLC**,** Hackensack, NJ) were loaded onto 1.3% denaturing agarose gel (Bio-rad, Hercules, CA), consisting of 1x MOPS buffer (Fisher, USA) and 5% solution of 37% formaldehyde (Fisher, USA), electrophoresed at 100V for 1h and transferred to positively-charged nylon membrane (Roche, Indianapolis, IN) using a Vacuum Blot System (Bio-Rad) transferring at 60mbar for 2 hours. To make RNA cross-linking solution, 245 µl of 12.5 M 1-methylimidazole (Sigma, St. Louis, MO) was suspended in 9 mL RNase free water, maintaining a pH of 8.0. Then, a total of 0.753 g 1-ethyl-3-(3-dimethylaminopropyl) carbodiimide (EDC) was added and the total volume adjusted to 24 mL with RNase-free water. RNA was then cross-linked to the membrane by placing the nylon membrane, side devoid of RNA, on saturated 3mm Whatman chromatography paper and incubating it in the freshly prepared EDC solution at 60°C for 2 hours. After cross-linking the membrane was washed with RNase-free water. Next, CjNC110-LNA probe (/5'DigN/ GCACATCAGTTTCAT/3'Dig_N/) (QIAGEN) was added to 15 mL DIG EasyHyb™ Buffer (Roche) to reach a final concentration of 25 ng/mL. Hybridization was performed using a hybridization oven and bottle, rotating at 42°C for 12 hours. After overnight incubation, subsequent washes and incubations were performed again using the hybridization chamber. The blot was first washed twice with low stringency buffer (2x SSC, 0.1% SDS) for 15 minutes at 50°C, and three times with high stringency buffer (0.1% SSC and 0.1% SDS) for 10 minutes at 50°C. DIG Washing and DIG Blocking Buffers were prepared using the DIG Wash and Block Set (Roche, USA). The blot was washed twice with Washing Buffer for 10 minutes at 37°C. Next, the blot was incubated in 1x Blocking Buffer for 3 hours at

room temperature. DIG antibody solution was added by mixing Blocking Buffer with DIG antibody at a ratio of 1:5,000. The blot was then incubated for 30 minutes at room temperature. Next, excess DIG antibody was removed by rinsing with the DIG Washing Buffer a total of four times for 15 minutes each. For development and detection, the membrane was placed in Development/Detection Buffer for 10 minutes, and 2 mL ready-to-use CDP-*Star*® (Roche, USA) was added to cover the blot completely. To image the blot, Chemidoc Imager (Bio-Rad) was used, exposing the blot for 5 minutes on the chemiluminescence setting. Image layout and annotations were performed using GraphPad Prism. ImageLab software (Bio-Rad) was used to generate a standard curve using RF and nt size of the ladder to predict the average band size of the target RNA.

TargetRNA2 and RNAFold

To attempt to computationally determine potential targets regulated by CjNC110 and to compare results to our RNAseq data, the freely available TargetRNA2 program (http://cs.wellesley.edu/~btjaden/TargetRNA2/) was utilized to predict potential targets of interest *a priori* [46]. The standard program settings were utilized, which included searching the region 80 nt upstream and 20 nt downstream of the predicted translational start site of all genes in the IA3902 genome. To attempt to predict the secondary structure of the CjNC110 non-coding RNA, the standard settings of the RNAFold webserver was used for prediction analysis (http://rna.tbi.univie.ac.at/cgi-bin/RNAfold.cgi) [47, 48]. Both the 137 nt read length predicted from Dugar *et al.* [21] and the 152 nt length predicted from our northern blot results were used for analysis via these methods.

Enumeration of *luxS* Transcriptional Levels Utilizing qRT-PCR

To validate the RNAseq results and compare *luxS* expression between mutants, quantitative reverse transcriptase PCR (qRT-PCR) was performed using total RNA isolated from IA3902 wild-type, ΔCjNC110, and ΔCjNC110c purified in three separate biological replicates of broth cultures grown to 12 hours from the second growth curve described above. Total RNA was extracted and qRT-PCR was performed using the iScript cDNA Synthesis Kit (Bio-Rad, Hercules, CA) and 1000 ng of total RNA according to the manufacturer's instructions as previously described [49]. Each sample was normalized to the same starting amount of cDNA using Qubit™ BR DNA Assay Kit (Invitrogen). cDNA purity was measured using the NanoDrop ND-1000 spectrophotometer. qPCR assays were run using the SsoAdvanced™ Universal SYBR® Green Supermix (Bio-Rad, Hercules, CA) and the CFX Maestro™ Real-Time PCR detection system (Bio-Rad). Dilutions of cDNA template for both standards and all unknowns were run in triplicate with reaction volumes of 10 µl. Amplification of converted cDNA occurred with 35 cycles of denaturation at 95°C for 10 seconds and then annealing for each primer pair (**Table 3**) at 58°C for 30 seconds. Prior to analysis, both standards curves (16S and *luxS*) were experimentally validated to have high efficiency 90%> of amplification and precision R^2=0.98 or greater. Relative fold change in *luxS* mRNA expression between IA3902 wild-type, ΔCjNC110, and ΔCjNC110c was calculated using the ISU Gallup Method Equation [50]. Statistical analyses was performed using one-way ANOVA (GraphPad Prism) to determine significance in gene expression levels. A p-value of <0.05 was considered significant.

Vibrio harveyi bioluminescence assay

Culture samples collected from time points 3, 6, 9 and 12 hours (2 mL each timepoint) from the second growth curve described above were centrifuged at 20,000 x *g* for 5 minutes at 4ºC. The supernatant was then removed from the cell pellet and filter-sterilized using a 0.2 µm syringe filter to create cell-free supernatant representative of the extracellular environment (E-CFS); both the E-CFS and the remaining cell pellet were then frozen at -80ºC. For processing of the cell pellet to create intracellular cell-free supernatant (I-CFS), samples were thawed on ice and then washed twice with PBS; following each wash, the cells were spun again at 8000 x *g* and the resulting supernatant was completely removed from the cell pellet. Next, the cell pellet was resuspended in 600 µl of ice-cold MH broth. The resuspended cell pellets were then lysed using a Bullet Blender® (NextAdvance, Troy, NY). To lyse the cells, 1.5 mL microcentrifuge tubes (Corning, Corning, NY) were loaded with sterilized 0.9-2.0 mm diameter stainless steel beads (NextAdvance). The Bullet Blender was used for 5 minutes at max speed and stored at 4°C. Lysed cellular debris were spun at 8000 x *g* for 2 minutes using a microcentrifuge, and the resulting supernatant filtered using a 0.20 µm sterile syringe filter, resulting in intracellular cell-free supernatant (I-CFS). Both E-CFS and I-CFS were frozen at -80 ºC until proceeding with the bioluminescence assay.

Autoinducer-2 levels within the collected supernatant for both intracellular (I-CFS) and extracellular (E-CFS) samples were then enumerated using the *Vibrio harveyi* bioluminescence assay as previously described [51]. Briefly, 10 µL of each CFS sample was added to 90 µL AB media containing a 1:5000 dilution of the reporter strain, *V. harveyi* strain BB170 [31] in triplicate. Relative light units (RLU) were measured every 15 minutes over 8 hours using the FLUOstar Omega (BMG Labtech, Ortenburg, Germany). MH broth and AB media were used as negative controls, while E-CFS collected from *V. harveyi* strain BB152 [29] was used as a positive control. The timepoints utilized for analysis were those occurring during the nadir of values for the negative control wells and at a standardized duration of time (approximately 3 hours) following initiation of increasing values for the positive wells. Results reported are the average of three independent growth curves with three technical replicates used at each timepoint. Statistical analysis was conducted using a two-way ANOVA with repeated measures and Sidak's multiple comparisons test (GraphPad Prism). A p-value of <0.05 was considered significant.

Motility assay

Motility was determined via inoculation of plates consisting of MH broth with 0.4% agar as previously described in our laboratory [8]. Briefly, the A_{600} of overnight cultures was adjusted to 0.3 using sterile MH broth on a Genesys 10S VIS spectrophotometer (Thermo Scientific™). A 1 µL volume inoculation stick was then dipped into a set volume of the standardized culture contained in the bottom of a 15 mL conical tube which was then used to make a stab inoculation into the center of the freshly made motility agar (MH broth with 0.4% Bacto agar) with a new inoculation stick for each plate. Plates were incubated at 42°C under microaerophilic conditions as described above with the exception that the plates were incubated right-side up and in a single layer. Measurement of the outermost reach of the halo was performed at 30 hours following inoculation for the first set of experiments and at 24 hours for the second set of experiments. All strains were assessed for average motility using six biological replicates consisting of six technical replicates during each independent study. The six experiments were statistically analyzed using a one-way ANOVA and differences between each strain assessed via Tukey's multiple comparisons test (GraphPad Prism). A p-value of <0.05 was considered significant.

Autoagglutination assay

Autoagglutination was assessed according to the method described previously [52] with some modifications. Briefly, the A_{600} of overnight cultures was adjusted to 1.0 in sterile Dulbecco's phosphate buffered saline (PBS) (Corning cellgro, Manassas, VA) using a Genesys 10S VIS spectrophotometer (Thermo Scientific™). The suspension was then aliquoted (2 mL each) into standard glass culture tubes. One subset of cultures were kept at controlled room temperature (25°C) under microaerophilic conditions; the others were incubated at 37°C microaerophilic. At 24 hours, 1 mL of the upper aqueous phase was carefully removed and A_{600} measured to determine autoagglutination activity. All strains were assessed in quadruplicate at each temperature in three independent experiments. The three experiments were statistically analyzed using a one-way ANOVA and differences between each strain assessed via Tukey's multiple comparisons test (GraphPad Prism). A p-value of <0.05 was considered significant.

Liquid Chromatography with Tandem Mass Spectrometry-Based Proteomic Analysis

For extraction of whole cell protein, bacterial cells from IA3902 wild-type, ΔCjNC110 and ΔCjNC110c were grown to exponential phase of growth at 16 hours on MH agar. Lawn cultures were then harvested from the plates using 1 mL of MH broth and resuspended in MH broth. Collected lawns were normalized to an A_{600} of 0.2 and aliquoted into 1 mL technical replicates. This was repeated for three biological replicates. To wash the cells, each aliquot was re-suspended in 1 mL of PBS, cells were spun down at 8000 x *g* for 3 minutes, and the supernatant was decanted. Next, 50 µl of lysis buffer (filtered sterilized water + 1% Triton X-100) was added to the protein pellets for resuspension (adapted from [53]). The cells were then mechanically sheared by boiling at 96°C for 5 minutes followed by rapid pipetting. After 3 cycles of boiling-shearing, total cell extracts were centrifuged at 10,000 × *g* for 5 min to remove cell debris. The supernatants were collected, and protein concentration was determined using the Qubit™ Protein Assay and Fluorometer (Invitrogen™). Crude protein was then submitted to the Iowa State Protein Facility. Crude protein extracts were digested overnight in solution with trypsin/Lys-C (25-50 µg). After digestion, Pierce™ Peptide Retention Time Calibration Mixture (PRTC) (ThermoFisher Scientific) was spiked into the samples to serve as an internal control (25 fmol/µL). The PRTC areas were used to normalize collision energies, retention times, and peak intensities to allow for quantitative analysis between samples.

Proteomic analysis was performed via liquid chromatography with tandem mass spectrometry (LC-MS/MS) using a Q Exactive™ Hybrid Quadrupole-Orbitrap Mass Spectrometer (Thermo Scientific™) system. The system was coupled with EASY-nLC 1200 nanopump with integrated auto-sampler (Thermo Scientific™). Liquid chromatography was used to separate the peptides followed by fragmentation and MS/MS analysis. The resulting intact fragmentation pattern was compared to a theoretical fragmentation pattern (MASCOT) to find peptides that can be used to identify high-confidence proteins. Minora Feature Detector was used for label-free quantification to detect and quantify discovered isotopic clusters.

Abundances of proteins were compared by grouping by strain and averaging the abundances of each protein identified. For data filtering and data imputation, PANDA-view, a freely available proteomic software (https://sourceforge.net/projects/panda-view/), was used [54]. Briefly, only proteins identified in two out of three biological replicates were included in

analysis. Nearest neighbor (kNN) imputation was used to fill any missing protein values [55]. All data was log transformed using $\log_2$. For statistical analysis, two-way ANOVA with false discovery rate correction set at 0.05 was performed (Graphpad Prism). Graphical Hierarchical clustering heat maps were generated using freely available MetaboAnalyst software [56]. The top 20 proteins were group and analyzed using the following heat map settings: distance measurement of Euclidean and the average clustering algorithm [56, 57].

Chicken colonization

Chicken colonization studies were performed as previously described in our laboratory utilizing 1 day-old broiler chicks obtained from a commercial hatchery [8]. A subset of chicks from each group were screened via cloacal swabs plated on MH agar containing both selective supplement and growth supplement (MH+sel+sup) (Oxoid, ThermoFisher Scientific) and found to be negative for *Campylobacter* carriage prior to inoculation. At 3 days of age, chicks were inoculated by oral gavage with 200 µl of bacterial suspension containing approximately 1×10^7 of one of the tested strains. Groups of chicks inoculated with specific strains were housed in separate brooders with no contact between the groups. At pre-determined timepoints post-inoculation (5 days, 12 days, and 19 days), a minimum of 5 chicks from each group were randomly selected for humane euthanasia which was immediately followed by necropsy. Cecal contents were harvested aseptically and stored on ice until further processing could be completed. Cecal samples were then weighed and subjected to a 10-fold serial dilution series, plated on MH+sel+sup agar, and grown under routine culture conditions as described above. To confirm that the isolates recovered were in fact the mutant strain and no cross contamination occurred, representative colonies were selected from each strain and timepoint, grown in MH+sel+sup broth, and plated on the respective antimicrobial selective agar of the mutant strain as described above. In addition, a minimum of two CFU from each group was collected for PCR analysis and confirmation of no cross-contamination between biological groups. The detection limit of the assay was determined to be 100 CFU/g; for isolates with no detectable colonies within the optimal target range of 30-300 CFU on the initial dilution plate, a count of 3×10^3 was used to enable statistical analysis. For statistical analysis, one-way ANOVA and Tukey's multiple comparison test was used to determine significant differences in colonization between biological groups (GraphPad Prism), using the null hypothesis that colonization rates between groups are the same. A p-value of <0.05 was considered significant.

Data availability

The RNAseq dataset generated in this publication has been deposited in the NCBI Database under BioProject ID Number PRJNA590513 (http://www.ncbi.nlm.nih.gov/bioproject/590513).

Results

Northern blotting and RNAseq validate expression of small RNA CjNC110 and mutant constructs

To validate expression of CjNC110 in IA3902, northern blots comparing IA3902 wild-type, ΔCjNC110 and ΔCjNC110c using 15 μg of total RNA extracted at log phase of growth from cultures collected at the same OD_{600} were performed. Northern blot analysis clearly demonstrates that small RNA CjNC110 is expressed by IA3902 wild-type and ΔCjNC110c but not ΔCjNC110 **(Fig 1)**. Using ImageLab, a standard curve was generated using RF and nt size of the ladder to predict the IA3902 CjNC110 average band size, which was 152bp. This is slightly larger than the size that was initially predicted in Dugar *et al.* which was 137bp [21].

Fig 1. Northern blotting demonstrates expression of CjNC110 in wild-type IA3902 and ΔCjNC110c but not in ΔCjNC110. Cultures for RNA extraction were collected at log phase of growth and northern blot analysis was conducted using 15 μg of total RNA in each of three separate lanes per strain tested.

The RNAseq data that was compiled for each of the mutants allowed further visualization of the unique read signature related to the mutated regions via the Integrated Genome Viewer as presented in **Fig 2A** and as compared to the anticipated mutated gene structure (**Fig 2B**). In all timepoints and replicates sequenced for the ΔCjNC110 and ΔCjNC110ΔluxS mutants, no reads mapped to the reported location of the CjNC110 small RNA; this was anticipated based on the method of mutant construction which removed that entire region of the genome en bloc and replaced it with an antibiotic resistance marker. Rockhopper did fail to identify CjNC110 as a small RNA candidate in this dataset which was somewhat unexpected. Further analysis of the data revealed that expression levels of CjNC110 transcripts were relatively low in the IA3902 wild-type at both stages of growth, which may explain why it was not recognized by Rockhopper as a unique ncRNA.

Fig 2. Graphic view of mutations. (A) A screen capture depicting the average RNAseq expression results from IGV of the *luxS* and CjNC110 regions of the genome, corresponding to the genome structure as depicted in (B) of all of the strains sequencing using RNAseq.

For the ΔluxS and ΔCjNC110ΔluxS mutants, the location of the insertion of the kanamycin resistance cassette into the coding sequence of the *luxS* gene can be directly observed as a sudden decrease in the amount of reads downstream of the location of the insert. In the ΔluxS mutant, reads mapping to CjNC110 can also be seen which indicates that the mutation does not interfere with ability of the downstream small RNA to be transcribed. In the ΔCjNC110ΔluxS mutant, no reads are present that map to the CjNC110 coding region, confirming that both genes are inactivated in that strain.

Differential gene expression analysis of RNAseq data indicates upregulation of *luxS* in ΔCjNC110 mutant and significant gene expression changes in ΔCjNC110Δ*luxS* associated with flagellar biosynthesis

Overall, 24 barcoded libraries were sequenced yielding over 109 million reads, with close to 100 million high quality reads aligning to either the genome or pVir plasmid of *C. jejuni* IA3902 and averaging 4,553,847 reads per library (**Tables C and D in S1 Appendix**). The vast majority of reads (average of 83% of total reads) mapped to protein coding genes of the

chromosome, with only 7% of reads mapping to ribosomal RNA on average following rRNA depletion with Ribo-Zero (median of 3%). Over half of the libraries contained less than or equal to 3% ribosomal RNA reads, which is consistent with the manufacturer's predicted rRNA removal efficiency. One third of the libraries did not exhibit efficient rRNA removal (>10% rRNA reads); the reason for this is unclear. Despite this difference in efficiency, all samples provided a more than adequate number of non-rRNA reads and thus were successfully utilized in the analysis. Less than 1% of reads mapped to antisense regions of the annotated genome.

A summary of the differences in numbers of genes with increased and decreased expression in the various strains and timepoints is given in **Table 2**, with a listing of specific genes given in **Table 3**. In the ΔCjNC110 mutant strain, six genes were found to be downregulated and four genes were found to be upregulated when compared to the IA3902 wild-type strain during exponential growth (complete information **Table E in S1 Appendix)**. In addition, a previously described non-coding RNA, CjNC140 [21] was found to be upregulated in the mutant condition. During the stationary phase, 16 genes were found to be downregulated and seven genes were found to be upregulated in the mutant strain when compared to wild-type. Of the regulated genes, three genes (*neuB2, hisF, ptmA*) were downregulated in the ΔCjNC110 mutant during both the exponential and stationary phases, and one hypothetical protein coding gene (CjSA_1261) was found to be upregulated in both conditions. Of the differentially expressed genes, five separate operons predicted by Rockhopper demonstrated multiple genes within the operon affected by the mutant condition. Analysis of functionality via the COG database revealed that multiple upregulated genes (*luxS, cetA, cetB*) were present in the "Signal transduction mechanisms" category; multiple downregulated genes were also included in the "Cell wall/membrane biogenesis" (*neuB2, ptmB,* CjSA_1352) category and "Posttranslational modification, protein turnover, chaperones" (*tpx,* CjSA_0687) functional category.

Table 2. Summary of differential gene expression results between mutant strains.

	Condition					
	ΔCjNC110		**ΔluxS**		**ΔCjNC110ΔluxS**	
	3 h	**12 h**	**3 h**	**12 h**	**3 h**	**12 h**
Protein-coding genes						
Number downregulated	6	16	1	6	61	32
Number upregulated	4	7	14	6	47	29
Non-coding RNA genes						
Number downregulated	0	0	0	0	25[b]	2
Number upregulated	1[a]	0	1[a]	0	1[a]	0

[a] = previously described ncRNA, CjNC140 [21]

[b] = 17 tRNA genes, 3 known RNA genes (tmRNA, SRP, 6S) and 4 newly predicted ncRNA

Table 3. Summary of differential gene expression (>1.5 fold change, q <0.05) in the IA3902 ΔCjNC110, ΔluxS and ΔCjNC110ΔluxS mutants as determined by RNAseq.

	Exponential (3 h)						Stationary (12 h)			
	ΔCjNC110*	**ΔluxS***	**ΔCjNC110ΔluxS***				**ΔCjNC110***	**ΔluxS***	**ΔCjNC110ΔluxS***	
Genes downregulated	*hisF*	CjSA_1350	CjSA_0014	*flgG*	*flgI*	*rplF*	*panC*	CjSA_0560	*rnhB*	*aroB*
	pseA		CjSA_0041	*mogA*	CjSA_1388	*rpsH*	CjSA_0559	CjSA_0620	CjSA_0158	CjSA_1137
	neuB2		*flgD*	*aspB*	CjSA_1389	*rpsN*	CjSA_0687	CjSA_1349	CjSA_0160	CjSA_1164
	ptmA		*flgE*	*hydD*	*flgK*	*rplE*	*Tpx*	CjSA_1350	CjSA_0284	*pyrH*
	CjSA_1352		CjSA_0067	*pseB*	*moaE*	*rplX*	CjSA_0785	*Acs*	*motB*	CjSA_1349
	rpsN		*accD*	*pseC*	*nuoD*	*rplN*	*ciaB*	*leuC*	*trpD*	CjSA_1350
			trxA	CjSA_1233	CjSA_1562	*rpmC*	CjSA_1102		CjSA_0344	CjSA_1414
			panB	*neuC2*	CjSA_1568	*rplP*	*petC*		CjSA_0372	*Acs*
			motB	CjSA_1350	CjSA_1577	CjSA_CjSRP1	CjSA_1137		CjSA_0389	CjSA_1461
			fliN	CjSA_1351	CjSA_t0035	CjSA_t0002	CjSA_1244		CjSA_0396	*rnhA*
			rpsU	CjSA_0788	CjSA_t0036	CjSA_t0005	*hisF*		*sdhA*	CjSA_1560
			frdB	*flgL*	CjSA_t0037	CjSA_t0007	*neuB2*		*sdhB*	*leuC*
			flag	*rpmH*	CjSA_t0038	CjSA_t0012	CjSA_1266		*uxaA*	*leuB*
			fliS	CjSA_0920	CjSA_t0039	CjSA_t0013	*ptmB*		CjSA_0560	*leuA*
			CjSA_0521	CjSA_1093	CjSA_t0043	CjSA_t0015	*ptmA*		CjSA_0616	CjSA_pVir0030
			CjSA_0569	CjSA_1102	CjNC130	CjSA_t0017	CjSAt0002		*trmD*	
			pstS	*dctA*	*secY*	CjSA_t0018				
			hslV	*luxS*	*rplO*	CjSA_t0020				
			flgH	CjSA_1182	*rpsE*	CjSA_t0021				
			flgG2	*porA*	*rplR*	CjSA_t0033				
Genes upregulated	CjSA_0008	*dnaN*	*dnaN*	*trpF*	*cetB*	CjSA_1449	*hcrA*	*flgE*	*dsbI*	CjSA_1107
	cetA	CjSA_0008	CjSA_0008	*trpB*	*cetA*	*rloH*	CjSA_0716	*flgG2*	CjSA_0040	*omp50*
	cetB	*trpF*	*gltD*	*trpA*	CjSA_1129	*nuoM*	CjSA_0717	*flgG*	CjSA_0041	CjSA_1180
	CjSA_1261	*trpB*	*folk*	CjSA_0337	CjSA_1131	CjSA_1549	CjSA_1107	*hcrA*	*flgD*	*pseB*
	CjNC140	CjSA_0337	CjSA_0076	CjSA_0370	CjSA_1145	*euC*	CjSA_1108	CjSA_1107	*flgE*	CjSA_1262
		CjSA_0370	CjSA_0105	CjSA_0372	CjSA_1164	*leuB,*	*omp50*	*nrfA*	*flgC*	*neuB2*
		CjSA_0732	CjSA_0110	*sdhA*	*cbpA*	*leuA*	*luxS*		*flgB*	*neuC2*
		CjSA_1017	*dgkA*	*sdhB*	CjSA_1259	CjNC140			*flgH*	*flgI*
		CjSA_1131	*pyrC*	CjSA_0490	CjSA_1260	CjSA_pVir0042			*flgG2*	CjSA_1387
		CjSA_1301	*Tal*	CjSA_0491	CjSA_1301	CjSA_pVir0044			*flgG*	*flgK*
		CjSA_1352	CjSA_0305	CjSA_0836	CjSA_1343	CjSA_pVir0025			*hcrA*	CjSA_1562
		CjSA_1449	*trpD*	*Cfa*	*tagF*				CjSA_0716	*p19*
		CjSA_1549							*flgS*	CjSA_pVir0042
		CjSA_pVir004							*flgL*	CjSA_pVir0013
		CjNC140							CjSA_0969	

* = additional small RNAs predicted by Rockhopper present with differential expression; see S4, S5, and S6 Tables for additional information

In the ΔluxS mutant strain, one gene was found to be downregulated and 14 genes were found to be upregulated when compared to the IA3902 wild-type strain during exponential growth (summary **Table 3**, complete information **Table F in S1 Appendix**). Similar to the ΔCjNC110 mutant, the previously described non-coding RNA CjNC140 was also found to be upregulated in the mutant condition during exponential growth only. At 12 hours, six genes were found to be downregulated and six upregulated in the ΔluxS mutant strain when compared to wild-type. Of the differentially expressed genes, only one gene, CjSA_1350, a putative methyltransferase, was found to be downregulated in the ΔluxS mutant during both exponential and stationary phases. Three separate operons predicted by Rockhopper demonstrated multiple genes within the operon affected by the mutant condition (two operons upregulated, one operon downregulated). Analysis of functionality via the COG database revealed that multiple both up- (*trpF, trpB*) and down- (CjSA_0620, *leuC*) regulated genes were present in the "Amino acid transport and metabolism" functional category; multiple upregulated genes were also included in the "Cell motility" (*flgE, flgG2, flgG*) functional category. Only two genes were differentially expressed in both the ΔCjNC110 and ΔluxS mutants, CjSA_0008 (upregulated during exponential growth hours) and CjSA_1107 (upregulated during stationary phase); both genes are annotated as hypothetical proteins at this time.

In the ΔCjNC110ΔluxS double knockout mutant, a large increase in both downregulated and upregulated genes when compared to wild-type was observed at both timepoints (summary **Table 3**, complete information **Table G in S1 Appendix**). Sixty-one protein coding genes, seventeen tRNA genes, three known ncRNA genes (tmRNA, SRP, 6S) and seven newly predicted ncRNAs were downregulated during exponential phase compared to IA3902 wild-type. In addition, 47 protein coding genes were upregulated in exponential phase, along with the previously described ncRNA CjNC140, which was also observed to be upregulated in the ΔCjNC110 and ΔluxS single knockout mutants. During stationary phase, 32 genes and two newly predicted non-coding RNAs were found to be downregulated, while 29 genes were upregulated in the mutant strain when compared to wild-type. Of the observed genes with differential expression, many were observed to show altered expression during both exponential and stationary phase when compared to wild-type; however, most were differentially expressed in the opposite direction between the two timepoints. Only two genes (*motB,* CjSA_1350) were downregulated in both conditions, while no genes were observed to be upregulated at both timepoints. Many of the differentially upregulated genes demonstrated in both background mutants, ΔCjNC110 and ΔluxS, were observed in the double knockout (**Figs 3A** and **3B**), while fewer of the downregulated genes were shared (**Figs 4A** and **4B**).

Fig 3. Venn diagram depicting the overlap of shared upregulated genes during the exponential and stationary growth phases. BioVenn was used to compare the lists of known genes upregulated in all 3 mutant strains during both exponential and stationary growth.

Fig 4. Venn diagram depicting the overlap of shared downregulated genes during the exponential and stationary growth phases. BioVenn was used to compare the lists of known genes downregulated in all 3 mutant strains during both exponential and stationary growth.

Of the differentially expressed genes affected by the ΔCjNC110ΔluxS double knockout mutation, 20 separate operons predicted by Rockhopper (predicted operon structure listed in **Table J in S2 Appendix**) demonstrated multiple genes within the operon affected by the mutant

condition (eight operons upregulated, four operons downregulated, and eight operons that showed opposing regulation at the different timepoints). **Figure A in S3 Appendix** shows the number of genes in each COG category that were differentially expressed in the double mutant condition during either exponential growth. The categories most affected by these mutations were "Energy production and conversion," "Amino acid transport and metabolism," "Translation," "Cell wall/membrane biogenesis," "Cell motility," and "Signal transduction mechanisms."

KEGG Pathways was used to determine the effect of the mutations on important pathways in *C. jejuni* pathobiology. **Figs 5A** and **5B** compare the genes observed to be differentially expressed in the double knockout mutant during both exponential and stationary phases for flagellar assembly. A large number of genes associated with flagellar assembly were noted to be differentially regulated in the double knockout mutant as compared to the single knockout mutants alone (**Fig C in S3 Appendix**).

Fig 5. KEGG Pathway analysis demonstrates alteration of expression of multiple genes involved in flagellar assembly in *C. jejuni* in the ΔCjNC110ΔluxS mutant during both exponential and stationary growth phases. Blue color indicates downregulation of gene expression, red color indicates up regulation of gene expression, green indicates that the gene is present in *C. jejuni* IA3902, and white indicates that the gene is not present in IA3902.

Identification of additional non-coding RNAs in IA3902

In addition to determining differential gene expression between the mutant and wild-type strains of IA3902, Rockhopper has the capability to predict non-coding RNAs present within the data. Prior to further manual analysis, Rockhopper predicted a total of 59 ncRNAs present in the data (57 chromosomal, 2 pVir). Of those 59, five align with previously identified ncRNAs (CjNC20, CjNC60, CjNC120, CjNC140, CJpv2), all of which were predicted to be conserved in IA3902 by Dugar *et al.* [21]. Manual curation of the list decreased the number of predicted ncRNA candidates to 40 (**Table H in S1 Appendix**). Candidate non-coding RNAs were discarded if they were related to the 16S or 23S genes as these were thought to be spuriously identified due to Ribo-Zero depletion differences between replicates; in addition, a single antisense RNA was discarded due to incorrect annotation of the *rnpB* gene to the wrong strand in IA3902. Of those remaining, 6 were demonstrated transcripts in the region of genes annotated as pseudogenes in IA3902 (CjSA1052, CjSA1323, CjSA1444, CjSA1543 and CjSA1630 – 2 separate ncRNA predictions). Two of the 40 remaining ncRNA candidates could potentially be classified as *cis* as they are transcribed opposite of transcribed regions of other genes; 25 would likely be considered *trans* ncRNAs as they are primarily located within intergenic regions; and seven are classified as anti-sense RNAs.

TargetRNA2 and RNAFold predictions suggest potential targets and secondary structure of CjNC110

The TargetRNA2 program predicted either 21 or 16 regulatory targets of CjNC110 in IA3902 based on the standard input parameters of the program and a 137 nt or 152 nt length, respectively (**Table I in S1 Appendix**). Of the predicted targets, only a single gene (CjSA_1137, annotated as an 2OG-Fe(II) oxygenase) was found to show significantly altered transcription in the CjNC110 mutant as compared to wild-type; this significant decrease was observed during

both exponential and stationary growth. This gene is located immediately downstream of CjNC110. No genes were noted to overlap with the protein expression data.

To assess secondary structure of the CjNC110, RNAFold was used to calculate the structure of CjNC110 using both the 137nt and 152nt predicted sizes, both of which yielded a prediction of a Y-shaped stem-loop structure (**Fig 6)**. When comparing the Target2RNA data to the RNAFold predictions, all of the predicted interaction areas of the non-coding RNA were grouped into the 3 unpaired loop regions of the RNA structure.

Fig 6. Structural prediction using RNAfold of the 137nt and 152 nt length options for CjNC110 RNA. For both the 137nt and 152nt predicted sizes, the structural prediction for CjNC110 contains 3 stem loops, with the unpaired loops being the region most likely to interact with mRNAs as predicted by TargetRNA2.

qRT-PCR confirms RNAseq results that *luxS* is transcribed at higher levels in ΔCjNC110 when compared to IA3902 wild-type

To further validate the results of the RNAseq and confirm that the increased expression of *luxS* in the ΔCjNC110 mutant was repeatable, qRT-PCR was performed on samples collected at 12 hours from the second growth curve using targets specific for the 3' region of the *luxS* gene. **Fig 7** demonstrates the expression levels of *luxS* in the ΔCjNC110 mutant compared to wild-type and confirms that increased *luxS* mRNA levels are present during stationary phase in the mutant, resulting in a fold change increase of 3.20 when compared to IA3902 wild-type. Additionally, ΔCjNC110c was tested to determine if complementation of the mutation returned *luxS* to wild-type levels; interestingly, ΔCjNC110c also demonstrated a fold change increase of 3.77 when compared to IA3902 wild-type. One-way ANOVA with Tukey's multiple comparison testing demonstrated significant fold change difference ($p < 0.05$) in *luxS* transcription between both ΔCjNC110 and ΔCjNC110c when compared to IA3902 wild-type.

Fig 7. qRT-PCR confirms *luxS* is transcribed at higher levels in the ΔCjNC110 and ΔCjNC110c backgrounds when compared to IA3902 wild-type (WT) (mean ± SEM). *C. jejuni* cultures were collected at timepoint 12 hours for RNA conversion cDNA for qRT-PCR to assesses expression of mRNA *luxS*. Each bar represents the average fold change expression from three biological replicates. Significance is denoted by "*" above each timepoint.

Growth of mutant strains during exponential growth is consistent with wild-type, but significant effects are seen in motility and autoagglutination

The growth of IA3902 wild-type, ΔCjNC110, ΔluxS, and ΔCjNC110ΔluxS was evaluated over a period of 30 hours and differences tested for statistical significance ($p < 0.05$) using two-way ANOVA with Dunnet's repeated measures of the A_{600} readings at each time point. ANOVA did identify a statistically significant difference between strains in both growth curves ($p < 0.05$), however, multiple comparison analysis of individual time points and strains when compared to wild-type growth revealed that the only significant difference was a decrease in the A_{600} of ΔCjNC110 after 27 and 30 hours in both growth curves performed (**Fig A in S3 Appendix** and **Fig 8)**. In both experiments, after 27 hours represents the point where a decline in the A_{600} begins to occur in all strains tested, and further examination of the actual CFU/mL over the course of

the first growth curve revealed that by 30 hours cell death was beginning to occur and colony counts were decreasing (**Fig A in S3 Appendix).** As further growth is assumed to be ceased at this time, there is likely minimal biological significance to the finding of differences after 27 hours in the assays performed using samples collected during exponential growth prior to 24 hours, however, there is possibly biological significance to the difference noted during the stationary phase which may warrant further investigation.

Fig 8. Shaking growth curve of wild-type IA3902 (WT) and isogenic mutants (mean ± SEM) confirm normal exponential growth. Results of four replicates (A_{600}) of a shaking growth curve performed in 250 mL Erlenmeyer flasks under microaerophilic conditions in MH broth. Samples were pulled from this growth curve and used for qRT-PCR and AI-2 bioluminescence assays. Significance is denoted by "*" above each timepoint.

Motility of the mutant strains in semi-solid agar was compared to wild-type IA3902 at 30 hours post-inoculation for all mutant isolates, and all isolates were confirmed to be highly motile (**Fig 9**). Statistical analysis via one-way ANOVA indicated that there was a significant difference between strains ($p < 0.0001$). Further post-hoc analysis via Tukey's multiple comparisons test did not reach statistical significance ($p > 0.05$) when comparing ΔCjNC110 to wild-type despite motility for the ΔCjNC110 strain observed to be consistently increased above the wild-type phenotype in all biological replicates performed. Results did reach statistical significance ($p < 0.05$), however, when comparing wild-type to both the ΔCjNC110ΔluxS and ΔluxS mutants which displayed statistically significant decreased motility; this result is consistent with previous reports of decreased motility of *luxS* mutants in the IA3902 background [8]. As many of the strains had migrated to the edge of the plate by 30 hours, we hypothesized that by reading the plates sooner we may observe a larger difference in the motility of the ΔCjNC110 strain, therefore, a second set of experiments was performed with measurements taken at 24 hours post-inoculation. When measured at 24 hours, motility for the ΔCjNC110 strain did demonstrate a statistically significant increase ($p < 0.05$) when compared to all other strains tested, and motility of both the ΔCjNC110ΔluxS and ΔluxS mutants was again noted to be significantly decreased. Following complementation of CjNC110, no significant difference was observed when compared to IA3902 wild-type in either experiment, confirming that complementation of CjNC110 quantitatively restored the phenotypic change back to wild-type levels.

Fig 9. Motility assays confirm isogenic mutants remain motile, with ΔluxS motility decreased and ΔCjNC110 motility increased over IA3902 wild-type (mean± SEM). Each bar represents the average motility of six biological replicates consisting of six technical replicates during each independent study. Significance is denoted by "*" above each bar when comparing wild-type to other respective strains at each independent timepoint.

Autoagglutination activity was measured at 25ºC and 37ºC following 24 hours of incubation (**Fig 10**) with an increase in optical density correlating to decreased autoagglutination ability, and a decrease in optical density correlating to increased autoagglutination ability. A statistically significant difference ($p < 0.0001$) between strains at both 25ºC and 37ºC was noted based on initial analysis via one-way ANOVA. When compared to IA3902 wild-type, autoagglutination activity for ΔluxS and ΔCjNC110ΔluxS was noted to be increased at a statistically significant level ($p < 0.05$) at both temperatures, while ΔCjNC110 exhibited

statistically significant decreased autoagglutination activity, again at both temperatures. Complementation of CjNC110 restored the autoagglutination ability of ΔCjNC110 to wild-type levels. These results indicate that *luxS* and CjNC110 function to influence autoagglutination activity in opposing directions; interestingly, when mutation of both genes was combined, the results favored the ΔluxS mutation but did return closer to wild-type levels.

Fig 10. ΔluxS bolsters autoagglutination and ΔCjNC110 hinders autoagglutination of IA3902 (mean± SEM). Autoagglutination as determined by optical density (A_{600}) was measured following a 24 hour incubation at either 25°C or 37°C. Each bar represents the average autoagglutination of 4 biological replicates consisting of 3 technical replicates during each independent study. Significance is denoted by "*" above each bar when comparing wild-type to other respective strains at each independent timepoint.

Vibrio harveyi bioluminescence assay demonstrates decreased extracellular AI-2 levels with a concomitant increase in intracellular AI-2 in ΔCjNC110

Bioluminescence activity was measured using the *Vibrio harveyi* assay as an approximation for extracellular (using E-CFS) AI-2 levels at various time points during the growth of IA3902 wild-type and mutant strains (**Fig 11A**). As expected, both the IA3902ΔluxS and ΔCjNC110ΔluxS mutant strains demonstrated no bioluminescence activity at any point during growth, indicating a complete lack of AI-2 production which is consistent with the absence of a functional LuxS protein. For the ΔCjNC110 mutant, bioluminescence was determined to be statistically significantly decreased when compared to wild-type at time points 6, 9 and 12 hours ($p < 0.05$) of the growth curve, occurring during mid to late exponential phase and early stationary phase. Complementation of ΔCjNC110 completely restored extracellular AI-2 to wild-type levels.

Fig 11. Bioluminescence activity as measured via the *Vibrio harveyi* bioassay over the course of growth (mean ± SEM) demonstrates (A) decreased extracellular AI-2 levels with (B) a concomitant increase in intracellular AI-2 in ΔCjNC110 Each bar represents the average RLU (AI-2 activity level) from three biological replicates consisting of three technical replicates each. Significance is denoted by "*" above each timepoint.

To determine if AI-2 production or transport across the cell membrane was impaired leading to this observed decrease in extracellular AI-2, the intracellular bioluminescence activity was also assessed utilizing I-CFS obtained from the cell pellet of the same culture as the E-CFS. Results of this assay demonstrated that intracellular AI-2 levels increased to statistically significant ($p < 0.05$) levels in the ΔCjNC110 mutant when compared to IA3902 wild-type at both the 9 hour and 12 hour timepoints. (**Fig 11B).** Again, complementation of ΔCjNC110 corrected the phenotypic alteration of increased intracellular AI-2 presence. These results indicate that the observed decrease in extracellular AI-2 activity is not due to impaired production, and instead suggests that transport of AI-2 across the cell membrane is altered in the ΔCjNC110 mutant.

Liquid Chromatography with Tandem Mass Spectrometry confirms increased LuxS protein abundance in both ΔCjNC110 and ΔCjNC110c

Proteomic analysis was conducted to reveal the most highly abundant proteins and changes in their translational level at exponential phase of growth to compare to transcriptomic data. Whole protein extract LC-MS/MS analysis resulted in a total of 262 identified proteins that were discovered in each biological group. Two-way ANOVA with FDR correction identified statistically significant differences in protein abundance; these proteins are illustrated in **Table 4**. When comparing wild-type to ΔCjNC110, proteins ThiJ and FrdA had a statistically significant fold change difference of 19.7 and -11.3, respectively. When comparing wild-type to ΔCjNC110c, proteins CjSA_0166 (lipoprotein) and RplN both had statistically significant fold change of -9.8, and RplU had a fold change of -4.9. In addition, proteins RecJ and AtpF demonstrated a statistically significant fold change of 8.0 and 9.2, respectively. There were several proteins that were identified as significantly different when comparing wild-type to both ΔCjNC110c and ΔCjNC110, including: LuxS, which exhibited increased expression, as well as CjSA_0067 (iron-sulfur protein) and CjSA_0489 (rhodanese-like domain-containing protein), both of which exhibited decreased expression in both backgrounds.

Table 4: Significant differentially expressed proteins identified from proteomic analysis ΔCjNC110 and ΔCjNC110c versus IA3902 wild-type

Protein ID	Geometric Mean (Abundance)		Fold Change vs WT	P-value*
	WT	Mutant		
ΔCjNC110				
CjSA_0067 - iron-sulfur protein	23726566.41	851708.3688	-27.9	<0.0001
CjSA_0489 - rhodanese-like domain-containing	35962749.77	2965820.801	-12.1	0.0001
ThiJ - thiazole monophosphate synthesis protein	1589344.014	31307392.07	19.7	<0.0001
FrdA - fumarate reductase flavoprotein subunit	3178688.029	280958.9826	-11.3	0.0002
LuxS - S-ribosylhomocysteine lyase	3913424.009	50859008.46	13.0	<0.0001
ΔCjNC110c				
CjSA_0067 - iron-sulfur protein	23726566.41	1123835.93	-21.1	<0.0001
CjSA_0489 - rhodanese-like domain-containing	35962749.77	2767208.654	-13.0	0.0001
CjSA_0166 – lipoprotein	25429504.23	2581896.969	-9.8	0.0006
RplN - 50S ribosomal protein L14	10327587.87	1048576	-9.8	0.0007
RplU - 50S ribosomal protein L21	15653696.03	3178688.029	-4.9	0.0007
RecJ - single-stranded-DNA-specific exonuclease	2408995.053	19271960.42	8.0	0.002
AtpF - ATP synthase subunit B	2965820.801	27254667.8	9.2	0.001
LuxS - S-ribosylhomocysteine lyase	3913424.009	54509335.6	13.9	<0.0001
CjSA_0926 - lipoprotein	1703416.738	23726566.41	13.9	0.0001

Geometric mean calculated by backtransforming log2 transformation value

*Two-way ANOVA FDR set at 0.05
WT = wild-type

Hierarchical heat maps also reveal contrasting protein expression patterns when comparing IA3902 wild-type to ΔCjNC110 and ΔCjNC110c. The top 20 hierarchical clustered proteins are illustrated for both ΔCjNC110 and ΔCjNC110c compared to wild-type IA3902 in **Fig 12**. Heat maps can provide meaningful clusters of data that can drive biomarker discovery that may not be picked up by a stricter statistical-based test, and can also shrink the data to find the most meaningful changes in the dataset. We note overlap between FDR significant proteins and proteins identified after heat map analysis, including ThiJ, LuxS, CJSA_0489, and CJSA_0166. Several additional proteins were identified via this approach that did not reach the FDR threshold for significance but exhibited clear differences in translational patterns when compared to IA3902 wild-type. In the ΔCjNC110 background, protein PycB demonstrated increased expression when compared to IA3902 wild-type, while proteins with decreased expression included CJSA_0387, CJSA_1389, NifU, FlaA, FlgD, and RpoZ. In addition, various proteins classified as periplasmic (CjSA_0190, CjSA_0854, CjSA_1107, CjSA_1178, CjSA1419, and CjSA1577) and lipoprotein (CjSA_0969) also exhibited decreased expression compared to wild-type. Complementation of the CjNC110 mutation resulted in reversal of these expression changes for all of the proteins described with the notable exception of LuxS which exhibited increased expression in both backgrounds; this finding was consistent with the results of the qPCR which demonstrated increased gene expression of *luxS* in both strains.

Fig 12. **Heatmaps reveal differential protein clustering patterns induced in both ΔCjNC110 and ΔCjNC110c when compared to IA3902 wild-type (WT).** All raw abundances were normalized, imputated, transformed to $\log_2$ scale values, and clustered based on resulting hierarchical patterns. The top 20 proteins were grouped and analyzed using heat map settings: distance measurement of Elucidean and average clustering algorithm.

Colonization of chickens is impaired in the ΔCjNC110 and absent in ΔluxS and ΔCjNC110ΔluxS mutants, but is restored to wild-type colonization levels in ΔCjNC110c

To determine if mutation of ΔCjNC110, ΔluxS and ΔCjNC110ΔluxS affected the ability of IA3902 to colonize chickens, cecal colonization levels were monitored for 3 weeks following oral inoculation of approximately 200 µl of $1x10^7$ CFU per strain. On DPI 5, a statistically significant decrease in colonization was noted for both the ΔCjNC110 and ΔluxS strains compared to wild-type; complementation of the ΔCjNC110 mutant restored colonization to wild-type levels (**Fig 13**). On DPI 12 and 19, a statistically significant decrease in colonization was noted for the ΔCjNC110, ΔluxS, and ΔCjNC110ΔluxS strains compared to wild-type with no colonization of ΔluxS and ΔCjNC110ΔluxS apparent at these time points; complementation of the ΔCjNC110 mutant again restored colonization levels to wild-type levels for both DPI 12 and 19. These results indicate that the presence of CjNC110 is necessary for optimal colonization, while *luxS* is required for colonization of IA3902 in chickens.

Fig 13. Chicken colonization is impaired in ΔCjNC110 and absent in ΔluxS and ΔCjNC110ΔluxS mutants compared to wild-type (mean ± SEM). Results are reported as $\log_{10}$ CFU/mL of ceca content for each sampling day [DPI 5 (Week 1), DPI 12 (Week 2), and DPI 19

(Week 3)]. Each bar represents the average colonization levels for each biological group with weekly technical replicates using a minimum of 6 birds. Significance is denoted by "*" above each timepoint.

Discussion

Over the past several years, RNAseq has become the method of choice to analyze the transcriptome of bacteria under various conditions as it allows evaluation of the entire transcriptome rather than only previously annotated regions as with older technology such as microarrays [58-60]. Recent work in *Campylobacter* has demonstrated that RNAseq can be useful for analyzing transcriptomic differences between wild-type and mutant strains following inactivation of protein-coding genes [61, 62]. In theory, RNAseq should also be able to be utilized for the same purpose of discovering the global effects of inactivation of ncRNAs. Small RNAs have been shown to be able to stabilize mRNA transcripts by multiple mechanisms [63], which should lead to increased levels of transcript availability and identification using RNAseq. In contrast, some interactions with ncRNAs have also been shown to increase transcript turnover by targeting transcripts for RNase degradation or exposing RNase cleavage sites [63], which should lead to decreased levels of transcripts available for identification via RNAseq. Thus, assessment of differential gene expression via RNAseq should be useful for uncovering interactions of ncRNAs with their targets that directly leads to altered levels of mRNA transcripts in the cell. One limitation of the use of RNAseq data for discovery of targets of small RNAs is that some target interactions may not lead to direct changes in mRNA transcript levels but instead affect the translation efficiency of the target mRNA; these types of interactions cannot be determined via this approach. Therefore, use of multiple additional methods such as computational approaches and proteomics to determine additional potential targets of ncRNAs is also warranted. The results of our work clearly indicate that RNAseq can be a useful tool for investigating the role of ncRNAs in gene expression in bacteria and can successfully be used to inform the design of phenotypic studies to begin to elucidate the function of ncRNAs in pathogenic bacteria.

During stationary phase in the ΔCjNC110 mutant, expression of the *luxS* mRNA was determined to be statistically significantly upregulated when compared to wild-type using RNAseq; during exponential growth, increased expression was also present but did not reach statistical significance. This initially suggested that CjNC110 may normally interact with the *luxS* transcript to impact AI-2 expression and quorum sensing. qRT-PCR confirmed the observed increase in *luxS* transcription seen via RNAseq, and increased expression of the LuxS protein was also observed via LC-MS/MS, clearly indicating that the response to the loss of CjNC110 expression was to increase LuxS protein production. However, further investigation revealed that despite the increased *luxS* expression and LuxS protein abundance in the CjNC110 mutant, AI-2 extracellular concentrations were decreased. This defect was corrected via complementation of CjNC110 despite the fact that *luxS* expression and LuxS protein abundance remained increased in the complement. The reason for the increased *luxS* expression and LuxS protein abundance in CjNC110c is currently unknown but is most likely related to additional unknown effects of CjNC110 on the AMC due to constitutive expression of CjNC110 in the complement. The increased *luxS* expression and LuxS protein abundance in the CjNC110c, combined with complementation back to wild-type of extracellular AI-2 activity, does clearly

demonstrate, however, that a change in LuxS protein abundance is not the cause of the observed difference in extracellular AI-2 concentrations.

Having ruled-out decreased LuxS abundance as a cause for the decreased extracellular AI-2, potential hypotheses for the observed difference included either decreased production of AI-2 by LuxS, increased degradation of AI-2, or altered kinetics of AI-2 movement into or out of the extracellular environment. To assess for altered kinetics of AI-2 movement, intracellular AI-2 levels were measured in the ΔCjNC110 mutant compared to wild-type and revealed an accumulation of AI-2 intracellularly in ΔCjNC110 that was corrected to wild-type levels in ΔCjNC110c. This indicates that impairment of AI-2 transport out of or increased import into the cell was the reason for the observed decrease in extracellular AI-2 in the CjNC110 mutant, and not decreased production or increased degradation. In *E. coli,* the YdgG (TqsA) protein, part of the AI-2 exporter superfamily, has been described to export AI-2 molecules [64]. To date, however, no similar homologue has been found in *C.jejuni*. Previous BlastP analysis has shown additional potential homologues of the YdgG protein exist within the *Campylobacterales* family, but none directly within the *C. jejuni* species [65]. Within our proteomics data, several periplasmic and lipoproteins which could be located in the cytoplasmic membrane were identified to exhibit decreased expression in ΔCjNC110 that was corrected to wild-type levels in ΔCjNC110c. The function of many of these proteins has yet to be elucidated in *Campylobacter,* therefore, future work assessing whether these proteins could serve as an AI-2 exporter in *C. jejuni* is warranted. In other species of bacteria such as *E. coli*, uptake of AI-2 from the extracellular environment has also been shown to be mediated by an active LSR system [66]. Comparative genomics has again failed to identify a homologous AI-2 uptake system in *C. jejuni*, however, several ABC-type transporters whose function remains to be elucidated do exist in *Campylobacter* sp. [27]. Several studies evaluating the concentration of AI-2 over time following addition of exogenous AI-2 to cell culture have attempted to determine whether or not AI-2 is able to be internalized in *C. jejuni* with mixed results [67, 68]. Thus, further research into an AI-2 uptake system in *C. jejuni* may also be warranted.

Interestingly, analysis of transcriptome changes in the ΔluxS mutant were not as enlightening as was expected. The list of genes identified does not overlap with the list of differentially expressed genes generated via microarray in *C. jejuni* strain 11168 which utilized the exact same mutant construct that was moved via homologous recombination into IA3902 [69]; however, differences in the strain of *C. jejuni* utilized in this study (IA3902) and culture conditions may explain why there was no overlap of differentially expressed genes. No genes associated with the AMC pathway were identified in our RNAseq data as have been previously reported via microarray in other strains of *C. jejuni* [70], however, there was very minimal expression of many of the genes associated with the AMC pathway in our data (*metE, metF, pfs*) which may have led to an inability to detect a difference. Decreased transcription of *flaA* has previously been associated with *luxS* mutation in strain 11168 [71]; expression of *flaA* during exponential growth was decreased 1.4-fold compared to wild-type, however, this change was not found to be statistically significant; no difference was present in *flaA* levels during stationary growth. A single gene, CjSA_1350, which is annotated as a putative methyltransferase, was found to be down-regulated during both exponential and stationary growth in the ΔluxS mutant of IA3902. The LuxS enzyme is critical for the formation of *S*-adenosylmethionine (SAM), which is a major methyl donor necessary for methylation of DNA, proteins, carbohydrates and other molecules important to the physiology of prokaryotes [72]. It is plausible that expression of this methyltransferase is sensitive to decreased availability of products from the activated methyl

cycle due to *luxS* mutation; however, recent data generated within our lab group suggests that this gene does not encode an active methyltransferase in IA3902 [73]. No change was detected in the expression of CjNC110 in the ΔluxS construct, however, an additional ncRNA, CjNC140, was noted to exhibit increased expression during exponential growth phase.

In distinct contrast to the lack of similar findings to previous studies exhibited by the IA3902ΔluxS mutant, when the ΔCjNC110 and ΔluxS mutations were combined into a double knockout mutant (ΔCjNC110ΔluxS), many of the previously noted transcriptional changes attributed to mutation of the *luxS* gene alone became apparent [70]. The He *et al.* [70] study was performed in a different strain of *C. jejuni*, 81-176, which also encodes and expresses CjNC110 [21]. After attempting to compare various strains and methods of mutation of the *luxS* gene and finding wide variation in phenotypical and transcriptional changes, Adler *et al.* [28] suggested that some of the differences reported between *luxS* mutants in various studies may be due to unknown polar affects caused by alteration of expression of CjNC110 based on the mutation strategy used for the *luxS* mutation. It seems highly likely based on the data generated in our study that some of the changes attributed to *luxS* mutation alone in the He *et al.* [70] study may in fact be due to inactivation of the CjNC110 transcript as well. Of the 57 genes listed as differentially expressed by the *luxS* mutant in He *et al.*[70], 21 were also found to be differentially expressed in our ΔCjNC110ΔluxS RNAseq data; again, none were found to be differentially expressed only in the ΔluxS mutant, while in contrast, three genes (*tpx, ptmB, ptmA*) were differentially expressed only in the ΔCjNC110 mutant. Of the 21 overlapping genes, only the flagellar genes *flgE, flgG2,* and *flgG* were differentially expressed in both the ΔluxS and ΔCjNC110ΔluxS mutants. These findings strongly suggest that in the previous study the main driver for the transcriptional changes seen was an inadvertent inactivation of both CjNC110 and *luxS,* and not *luxS* alone. Of the genes identified in both our study and He *et al.* [70], a large number of the hook-basal body associated proteins (FlgD, FlgE, FlgG, FlgG2, FlgH, FlgI, and FlgK) that are under the control of σ^{54} (RpoN) promotors [74, 75] were identified. Expression from σ^{54} promotors has been shown to require activation of the FlgRS two-component regulatory system [74, 76]. Many of these showed opposite differences based on growth phase (decreased exponential, increased stationary), and it has been previously demonstrated that regulation by these sigma-factors is growth cycle dependent, with σ^{54}-regulated genes typically expressed between σ^{70}- and σ^{28}-associated genes [74], which may help explain the differences seen here. Of particular note is the fact that *flgS* was observed to be upregulated in the ΔCjNC110ΔluxS mutant. It has been previously suggested that an additional unknown factor may control the temporal regulation of σ^{54} dependent flagellar genes [77]; therefore, it is reasonable to consider based on our results that *luxS* or CjNC110 may play a role in this regulation.

Several additional phenotypes of interest were identified in our research, including alteration of the ability to colonize chickens by ΔCjNC110, ΔluxS and ΔCjNC110ΔluxS. The abolishment of the ability of ΔluxS to colonize chickens has previously been described in IA3902 but not in NCTC 11168; the reason for this difference is currently unknown, but has been speculated to be related to strain-specific differences in the metabolism of methionine or *S*-adenosylmethionine (SAM) recycling which are also affected by the *luxS* mutation [27]. Additional work in our lab has shown that the *luxS* mutation in IA3902 does disrupt the AMC, which functions to recycle SAM and produce methionine [49], however, DNA methylation in IA3902 was not affected by the *luxS* mutation [73]. Comparative genomics reveals that NCTC 11168 does harbor an additional genomic system for methionine biosynthesis in the form of *metAB* which is not present in IA3902 and may represent an alternative pathway for synthesis of

this required amino acid and an explanation for the observed difference in colonization ability. Mutation of ΔCjNC110 in our work also led to a significantly decreased colonization ability in IA3902 compared to wild-type, indicating that this ncRNA has the potential to play a key role in modulating colonization by *C. jejuni*. Further work is ongoing in our lab to determine if mutation of CjNC110 in NCTC 11168 also displays a colonization defect, or, if similar to *luxS*, the phenotype differs from IA3902.

Motility is considered critical for the *in vivo* virulence of *C. jejuni* and requires a functional flagellar apparatus [78, 79]; however, this alone is not sufficient for normal motility to be present [80]. In our study, a statistically significant increase in motility was found between the ΔCjNC110 mutant and wild-type when motility was assessed at 24 hours rather than 30 hours. Interestingly, when assessing the transcriptomics data, the *cetAB* operon (*Campylobacter* energy taxis proteins A and B), which is known to mediate energy taxis response in *Campylobacter* [81], was statistically significantly upregulated in the ΔCjNC110 mutant when compared to wild-type during the exponential phase of growth. Expression of *cetAB* was increased during the stationary phase as well, however, did not reach the level of statistical significance. Defects in both *cetA* and *cetB* have been shown to lead to altered motility phenotypes, particularly in response to migration towards critical factors in *Campylobacter* metabolism such as sodium pyruvate and fumarate [80]. Investigation of expression of *cetA* and *cetB* has shown that levels of the gene products are unaffected by mutation of sigma factors σ^{54} or σ^{28}, indicating that transcription of the *cetAB* operon is likely controlled by σ^{70} or another yet unknown transcription factor [81]. Based on this information, it seems plausible that CjNC110 might normally act as a repressor of the CetAB energy taxis system. Attempts to determine the location of the interaction between the *cetAB* operon and CjNC110 using computational prediction programs such as TargetRNA2 failed to identify an interaction region, however, computational methods of target identification are particularly unrewarding in non-model organisms such as *Campylobacter* due to a lack of conservation of small RNAs in these species [18]. Our proteomics data also failed to detect the CetA and CetB proteins, therefore, we could not validate that increased expression of *cetA* and *cetB* resulted in increased protein expression levels. Many of the proteins identified in our study exhibited extremely high expression levels, which, without fractioning, prevented proteins of lesser abundance from being detected. Whole cell proteomic analysis with fractioning and time-course analysis would be required to reveal the entire proteomic network regulated by CjNC110 and validate expression patterns of proteins of lesser abundance than the 262 proteins that were identified in our study. Further work to determine if an interaction between CjNC110 and the *cetAB* operon exists and leads to increased expression of the CetA and CetB proteins is warranted.

Minimal changes in genes associated with the flagellar apparatus were noted in the transcriptome of ΔCjNC110 which may also help to explain why an increase in energy taxis would allow for an increase in observed motility with the assumption that normally functioning flagella are present. In contrast to the ΔCjNC110 strain, however, both the ΔluxS and ΔCjNC110ΔluxS mutants did display altered expression of genes associated with the flagellar apparatus during at least one stage of growth. For the ΔluxS mutant, a small number of flagellar associated genes were observed to be upregulated during stationary growth. No additional genes known to be related to motility in *C. jejuni* appeared to be affected by the *luxS* mutation; therefore, a reasonable explanation for the decreased motility cannot be ascertained from this data alone. For the ΔCjNC110ΔluxS mutant, however, there were a large number of genes involved in assembly of the flagellar apparatus that demonstrated dysregulation when both the

luxS and CjNC110 mutations were combined. Many genes related to flagellar assembly were decreased in expression during exponential growth; however, the same genes were increased in expression during stationary growth. Our data in this study demonstrated a statistically significant decrease in motility of the ΔCjNC110ΔluxS mutant when compared to both wild-type and the ΔCjNC110 mutant. This suggests that the decrease in motility is unrelated to the CjNC110 mutation when present by itself, but when both the ΔluxS and ΔCjNC110 mutations are combined, the effect of decreased motility observed in the *luxS* mutation is maintained.

The presence of normal flagella has also been associated with autoagglutination ability and is considered necessary but not sufficient for this important trait [80]. Previous studies in *C. jejuni* have demonstrated that interactions between modifications on adjacent flagellar filaments, particularly those provided by protein glycosylation, are required for normal autoagglutination ability [82]. In addition, mutants defective in autoagglutination ability have also been shown to display a decrease in adherence and invasion ability *in vitro* as well as attenuation in disease models [82]. In the present study, the ΔCjNC110 mutant exhibited decreased autoagglutination when compared to wild-type at both 25ºC and 37ºC. Interestingly, two genes that have been associated with flagellar glycosylation, *ptmA* and *neuB2*, were downregulated in our RNAseq data in the ΔCjNC110 mutant when compared to wild-type during both exponential and stationary growth phases. The *ptmA* and *neuB2* genes have been previously shown to be involved in production of Leg5Am7Ac and PseAm, two important structural glycans involved in flagellar glycosylation in *C. jejuni* [83, 84]. A decrease in the amount of flagellar glycosylation related to decreased production of these genes could in theory lead to decreased autoagglutination ability. The fact that we observed a decrease in autoagglutination activity in the ΔCjNC110 mutant, combined with RNAseq data indicating a decrease in the presence of the mRNA transcripts of the genes *ptmA* and *neuB2* that affect flagellar glycosylation, suggests that these findings represent a true phenotypic change in the CjNC110 mutant and an additional potential area of regulation for the CjNC110 non-coding RNA. In this case, and in contrast to the *cetAB* operon where removal of CjNC110 led to an increase in expression, inactivation of CjNC110 led to a decrease in the expression of these two genes which were predicted to belong to the same operon in our Rockhopper analysis. In other bacterial species, small ncRNAs have been shown to lead to stabilization of the target mRNA [85]. This suggests that CjNC110 may normally serve in *trans* to prevent degradation of the *ptmA* and *neuB2* mRNA transcripts after they have been produced, leading to increased longevity of the mRNA and thus increasing levels of the translated protein. By removing CjNC110, stabilization of the mRNA message of *ptmA* and *neuB2* may not occur as normal, leading to increased turnover of the message and decreased protein production. Again, attempts to determine the location of the interaction between *ptmA*, *neuB2* and CjNC110 using computational prediction programs such as TargetRNA2 failed to identify an interaction region, and our proteomics data failed to identify either protein.

In contrast to ΔCjNC110, the ΔluxS mutant exhibited statistically significant increased autoagglutination at both 25°C and 37°C. This finding is the opposite of what was observed in a different strain of *C. jejuni*, 81-176, where the *luxS* mutation led to a decrease in autoagglutination ability [71]. Mutation of the *luxS* gene by Jeon *et al.* [71] was accomplished using the same method as He *et al.* [70], thus it is plausible that the results obtained may also be a result of the *luxS* gene inactivation in combination with polar affects to CjNC110. However, there are also known differences between strains of *C. jejuni* in the type of flagellar glycosylation present, particularly between NCTC 11168 (considered sytenic to IA3902) and 81-176, which may help to further explain the differences observed between autoagglutination studies

performed using different *C. jejuni* strains [86]. It is unclear at this time what mechanism allowed for increased autoagglutination ability in the ΔluxS mutant in this particular strain of *C. jejuni*. In addition, while these changes in autoagglutination are statistically significant, the biological relevance at this time is unknown, particularly as decreased to absent colonization of chickens was again confirmed in this mutant. When measured in terms of percent of normal autoagglutination of the IA3902 wild-type strain, for the ΔluxS mutant, autoagglutination ability was observed to be 172% and 168% of the wild-type at 25°C and 37°C, respectively. For the ΔCjNC110 mutant, autoagglutination was observed to be 53% at 25°C and 56% at 37°C of the wild-type. Following complementation of CjNC110, on a percentage basis autoagglutination levels were much closer to wild-type demonstrating autoagglutination activity of 101% at 25ºC and 107% at 37ºC. However, when compared to the percentage of autoagglutination possible, which would be considered 100% at an A_{600} of 0.00 and 0% at an A_{600} of 1.0, both the wild-type and mutant strains still exhibited a relatively high ability to autoagglutinate**.** For comparison, mutations in the *flaA/flaB* and *flbA* genes of *C. jejuni* strain 81-176 led to a decrease from A_{600} 0.031 (96.9%) to 0.731 (24.9%) and 0.654 (35.6%), respectively [52]. While not reflected in the transcriptomic data, our proteomic heat map data did show a decrease in FlaA translation in ΔCjNC110, thus it is possible that the decreased autoagglutination observed in this mutant may also be related to a decrease in FlaA protein abundance [52]. Differences in virulence displayed in both *in vitro* and *in vivo* models are likely to be expected with such dramatic changes in AAG activity as displayed in the *flaA/flab* and *flbA* mutations. As neither the *luxS* gene nor the CjNC110 are known to be directly involved in flagellar glycosylation, it seems reasonable that inactivation of these genes could lead to a modification of autoagglutination ability without complete loss or gain of function. Further work including assessment for changes in the flagellar glycosylation of these mutants when compared to the IA3902 wild-type and additional *in vitro* and *in vivo* analysis of flagellar glycosylation is warranted.

Several additional putative ncRNAs were also identified via the Rockhopper program which allowed for confirmation of expression of five non-coding RNAs conserved among *Campylobacter* species that were previously predicted to be present in IA3902 [21]. The majority of the other identified putative non-coding RNAs that were predicted by the program have not been previously reported in *C. jejuni.* Based on the data presented in Dugar *et al.* [21] that suggests that many small RNAs in *Campylobacter* are strain-specific, the fact that the predicted RNAs were not previously identified does not mean that they are not real. That being said, there are limitations to the identification of non-coding RNAs by Rockhopper. One-third of the initially predicted ncRNAs were manually discarded as they mapped to the region of the 16S or 23S genes and were likely identified due to differences between replicates in Ribo-Zero rRNA depletion efficiency. Another subset of the identified non-coding RNAs were recognized by the program because the genome file utilized by Rockhopper does not include pseudogenes, therefore, reads that mapped to areas of putative pseudogenes were classified as non-coding RNA. While it is possible that these transcripts no longer serve as functional mRNA transcripts and now instead act as functional non-coding RNAs, it is probably more likely that these transcripts either do form functional proteins or are simply a non-functional remnant of what once was a functional protein-coding message.

While not explored further in our phenotypic studies, Rockhopper did identify two additional non-coding RNAs, CjNC140 and CjNC130/6S, as being differential expressed in our mutants; these ncRNAs have been previously identified and confirmed to be transcribed in multiple other *Campylobacter* species [21]. Of particular interest is the CjNC140 non-coding

RNA. Predicted to be transcribed in the intergenic region upstream of *porA*, this ncRNA was upregulated during exponential growth in all three of the mutant strains when compared to wild-type (**Fig D in S3 Appendix**). As increased expression was not observed during stationary growth, this suggests that CjNC140 may serve as a regulator involved in mediating changes during different stages of bacterial growth. The fact that its expression is similarly altered under all 3 mutant conditions also suggests that the three genes, *luxS*, CjNC110 and CjNC140, may normally interact within the cell in some way to facilitate these changes. Point mutations in the nearby *porA* have also been recently determined to be sufficient to cause the abortion phenotype [10], making this ncRNA particularly interesting for further study. Futher work is ongoing in our lab to determine the role of CjCN140 in the pathophysiology of *C. jejuni* as well.

Conclusion

The results of our research clearly demonstrate a significant role for CjNC110 in the pathobiology of *C. jejuni* IA3902. The collective results of the phenotypic and transcriptomic changes observed in our data complement each other and suggest that CjNC110 may be involved in regulation of energy taxis, flagellar glycosylation, cellular communication via quorum sensing, and chicken colonization in *C. jejuni* IA3902. This work provides for the first time valuable insights into the potential regulatory targets of the CjNC110 small RNA in the zoonotic pathogen *C. jejuni* and suggests a wide range of research avenues into the role of non-coding RNAs in the pathobiology of this important zoonotic pathogen.

Acknowledgements

The authors would like to thank Dr. Lei Dai and Dr. Zuowei Wu for technical assistance in mutant construction and northern blot technique.

References

1. World Health Organization. WHO estimates of the global burden of foodborne diseases: foodborne disease burden epidemiology reference group 2007-2015. 2015 [cited 2015 December 3]. Available from: http://apps.who.int/iris/bitstream/10665/199350/1/9789241565165_eng.pdf.

2. Sahin O, Plummer PJ, Jordan DM, Sulaj K, Pereira S, Robbe-Austerman S, et al. Emergence of a tetracycline-resistant Campylobacter jejuni clone associated with outbreaks of ovine abortion in the United States. J Clin Microbiol. 2008;46(5):1663-71. Epub 2008/03/07. doi: JCM.00031-08 [pii]10.1128/JCM.00031-08. PubMed PMID: 18322054; PubMed Central PMCID: PMC2395063.

3. Sahin O, Fitzgerald C, Stroika S, Zhao S, Sippy RJ, Kwan P, et al. Molecular evidence for zoonotic transmission of an emergent, highly pathogenic Campylobacter jejuni clone in the United States. J Clin Microbiol. 2012;50(3):680-7. Epub 2011/12/23. doi: JCM.06167-11 [pii]

10.1128/JCM.06167-11. PubMed PMID: 22189122; PubMed Central PMCID: PMC3295108.

4. Tang Y, Meinersmann RJ, Sahin O, Wu Z, Dai L, Carlson J, et al. Wide but Variable Distribution of a Hypervirulent Campylobacter jejuni Clone in Beef and Dairy Cattle in the United States. Appl Environ Microbiol. 2017;83(24). doi: 10.1128/AEM.01425-17. PubMed PMID: 28970227; PubMed Central PMCID: PMCPMC5717212.

5. Wu Z, Sahin O, Shen Z, Liu P, Miller WG, Zhang Q. Multi-omics approaches to deciphering a hypervirulent strain of Campylobacter jejuni. Genome biology and evolution. 2013;5(11):2217-30. doi: 10.1093/gbe/evt172. PubMed PMID: 24201373; PubMed Central PMCID: PMC3845652.

6. Grogono-Thomas R, Blaser MJ, Ahmadi M, Newell DG. Role of S-layer protein antigenic diversity in the immune responses of sheep experimentally challenged with Campylobacter fetus subsp. fetus. Infect Immun. 2003;71(1):147-54. PubMed PMID: 12496160; PubMed Central PMCID: PMC143156.

7. van Putten JP, van Alphen LB, Wosten MM, de Zoete MR. Molecular mechanisms of campylobacter infection. Current topics in microbiology and immunology. 2009;337:197-229. doi: 10.1007/978-3-642-01846-6_7. PubMed PMID: 19812984.

8. Plummer P, Sahin O, Burrough E, Sippy R, Mou K, Rabenold J, et al. Critical role of LuxS in the virulence of Campylobacter jejuni in a guinea pig model of abortion. Infect Immun. 2012;80(2):585-93. Epub 2011/12/07. doi: IAI.05766-11 [pii]10.1128/IAI.05766-11. PubMed PMID: 22144479; PubMed Central PMCID: PMC3264297.

9. Sahin O, Terhorst SA, Burrough ER, Shen Z, Wu Z, Dai L, et al. Key Role of Capsular Polysaccharide in the Induction of Systemic Infection and Abortion by Hypervirulent Campylobacter jejuni. Infect Immun. 2017;85(6). doi: 10.1128/IAI.00001-17. PubMed PMID: 28373351; PubMed Central PMCID: PMCPMC5442617.

10. Wu Z, Periaswamy B, Sahin O, Yaeger M, Plummer P, Zhai W, et al. Point mutations in the major outer membrane protein drive hypervirulence of a rapidly expanding clone of Campylobacter jejuni. Proc Natl Acad Sci U S A. 2016;113(38):10690-5. doi: 10.1073/pnas.1605869113. PubMed PMID: 27601641; PubMed Central PMCID: PMCPMC5035848.

11. Parkhill J, Wren BW, Mungall K, Ketley JM, Churcher C, Basham D, et al. The genome sequence of the food-borne pathogen Campylobacter jejuni reveals hypervariable sequences. Nature. 2000;403(6770):665-8. doi: 10.1038/35001088. PubMed PMID: 10688204.

12. Papenfort K, Vogel J. Regulatory RNA in bacterial pathogens. Cell host & microbe. 2010;8(1):116-27. doi: 10.1016/j.chom.2010.06.008. PubMed PMID: 20638647.

13. Storz G, Vogel J, Wassarman KM. Regulation by small RNAs in bacteria: expanding frontiers. Molecular cell. 2011;43(6):880-91. doi: 10.1016/j.molcel.2011.08.022. PubMed PMID: 21925377; PubMed Central PMCID: PMC3176440.

14. Caldelari I, Chao Y, Romby P, Vogel J. RNA-mediated regulation in pathogenic bacteria. Cold Spring Harbor perspectives in medicine. 2013;3(9):a010298. doi: 10.1101/cshperspect.a010298. PubMed PMID: 24003243.

15. Beisel CL, Storz G. Base pairing small RNAs and their roles in global regulatory networks. FEMS microbiology reviews. 2010;34(5):866-82. doi: 10.1111/j.1574-6976.2010.00241.x. PubMed PMID: 20662934; PubMed Central PMCID: PMC2920360.

16. Sharma CM, Hoffmann S, Darfeuille F, Reignier J, Findeiss S, Sittka A, et al. The primary transcriptome of the major human pathogen Helicobacter pylori. Nature. 2010;464(7286):250-5. Epub 2010/02/19. doi: nature08756 [pii]10.1038/nature08756. PubMed PMID: 20164839.

17. Valentin-Hansen P, Eriksen M, Udesen C. The bacterial Sm-like protein Hfq: a key player in RNA transactions. Mol Microbiol. 2004;51(6):1525-33. PubMed PMID: 15009882.

18. Livny J, Teonadi H, Livny M, Waldor MK. High-throughput, kingdom-wide prediction and annotation of bacterial non-coding RNAs. PLoS One. 2008;3(9):e3197. doi: 10.1371/journal.pone.0003197. PubMed PMID: 18787707; PubMed Central PMCID: PMC2527527.

19. Chaudhuri RR, Yu L, Kanji A, Perkins TT, Gardner PP, Choudhary J, et al. Quantitative RNA-seq analysis of the Campylobacter jejuni transcriptome. Microbiology. 2011;157(Pt 10):2922-32. Epub 2011/08/06. doi: mic.0.050278-0 [pii]10.1099/mic.0.050278-0. PubMed PMID: 21816880; PubMed Central PMCID: PMC3353397.

20. Butcher J, Stintzi A. The transcriptional landscape of Campylobacter jejuni under iron replete and iron limited growth conditions. PLoS One. 2013;8(11):e79475. doi: 10.1371/journal.pone.0079475. PubMed PMID: 24223952; PubMed Central PMCID: PMC3815106.

21. Dugar G, Herbig A, Forstner KU, Heidrich N, Reinhardt R, Nieselt K, et al. High-resolution transcriptome maps reveal strain-specific regulatory features of multiple Campylobacter jejuni isolates. PLoS Genet. 2013;9(5):e1003495. Epub 2013/05/23. doi: 10.1371/journal.pgen.1003495PGENETICS-D-13-00603 [pii]. PubMed PMID: 23696746; PubMed Central PMCID: PMC3656092.

22. Porcelli I, Reuter M, Pearson BM, Wilhelm T, van Vliet AH. Parallel evolution of genome structure and transcriptional landscape in the Epsilonproteobacteria. BMC Genomics. 2013;14(1):616. Epub 2013/09/14. doi: 1471-2164-14-616 [pii]10.1186/1471-2164-14-616. PubMed PMID: 24028687.

23. Taveirne ME, Theriot CM, Livny J, Dirita VJ. The Complete Campylobacter jejuni Transcriptome during Colonization of a Natural Host Determined by RNAseq. PLoS One. 2013;8(8):e73586. Epub 2013/08/31. doi: 10.1371/journal.pone.0073586PONE-D-13-20915 [pii]. PubMed PMID: 23991199; PubMed Central PMCID: PMC3749233.

24. Kreuder AJ, Schleining JA, Yaeger M, Zhang Q, Plummer PJ. RNAseq Reveals Complex Response of Campylobacter jejuni to Ovine Bile and In vivo Gallbladder Environment. Front Microbiol. 2017;8:940. doi: 10.3389/fmicb.2017.00940. PubMed PMID: 28611744; PubMed Central PMCID: PMCPMC5447181.

25. Le MT, van Veldhuizen M, Porcelli I, Bongaerts RJ, Gaskin DJ, Pearson BM, et al. Conservation of sigma28-Dependent Non-Coding RNA Paralogs and Predicted sigma54-Dependent Targets in Thermophilic Campylobacter Species. PLoS One. 2015;10(10):e0141627. doi: 10.1371/journal.pone.0141627. PubMed PMID: 26512728; PubMed Central PMCID: PMC4626219.

26. Shen Z, Patil RD, Sahin O, Wu Z, Pu XY, Dai L, et al. Identification and functional analysis of two toxin-antitoxin systems in Campylobacter jejuni. Mol Microbiol. 2016;101(6):909-23. doi: 10.1111/mmi.13431. PubMed PMID: 27291507.

27. Plummer PJ. LuxS and quorum-sensing in Campylobacter. Front Cell Infect Microbiol. 2012;2:22. doi: 10.3389/fcimb.2012.00022. PubMed PMID: 22919614; PubMed Central PMCID: PMCPMC3417632.

28. Adler L, Alter T, Sharbati S, Golz G. Phenotypes of Campylobacter jejuni luxS mutants are depending on strain background, kind of mutation and experimental conditions. PLoS One. 2014;9(8):e104399. doi: 10.1371/journal.pone.0104399. PubMed PMID: 25093839; PubMed Central PMCID: PMC4122453.

29. Bassler BL, Wright M, Showalter RE, Silverman MR. Intercellular signalling in Vibrio harveyi: sequence and function of genes regulating expression of luminescence. Mol Microbiol. 1993;9(4):773-86. PubMed PMID: 8231809.

30. Plummer P, Zhu J, Akiba M, Pei D, Zhang Q. Identification of a key amino acid of LuxS involved in AI-2 production in Campylobacter jejuni. PLoS One. 2011;6(1):e15876. Epub 2011/01/26. doi: 10.1371/journal.pone.0015876. PubMed PMID: 21264316; PubMed Central PMCID: PMC3019222.

31. Bassler BL, Wright M, Silverman MR. Multiple signalling systems controlling expression of luminescence in Vibrio harveyi: sequence and function of genes encoding a second sensory pathway. Mol Microbiol. 1994;13(2):273-86. PubMed PMID: 7984107.

32. Wang Y, Taylor DE. Chloramphenicol resistance in Campylobacter coli: nucleotide sequence, expression, and cloning vector construction. Gene. 1990;94(1):23-8. PubMed PMID: 2227449.

33. Gibson DG, Young L, Chuang RY, Venter JC, Hutchison CA, 3rd, Smith HO. Enzymatic assembly of DNA molecules up to several hundred kilobases. Nature methods. 2009;6(5):343-5. doi: 10.1038/nmeth.1318. PubMed PMID: 19363495.

34. Wang Y, Taylor DE. Natural transformation in Campylobacter species. J Bacteriol. 1990;172(2):949-55. PubMed PMID: 2404960; PubMed Central PMCID: PMC208523.

35. Kim SW, Li Z, Moore PS, Monaghan AP, Chang Y, Nichols M, et al. A sensitive non-radioactive northern blot method to detect small RNAs. Nucleic Acids Res. 2010;38(7):e98. doi: 10.1093/nar/gkp1235. PubMed PMID: 20081203; PubMed Central PMCID: PMCPMC2853138.

36. Muraoka WT, Zhang Q. Phenotypic and genotypic evidence for L-fucose utilization by Campylobacter jejuni. J Bacteriol. 2011;193(5):1065-75. Epub 2011/01/05. doi: JB.01252-10 [pii]10.1128/JB.01252-10. PubMed PMID: 21193610; PubMed Central PMCID: PMC3067607.

37. Karlyshev AV, Wren BW. Development and application of an insertional system for gene delivery and expression in Campylobacter jejuni. Appl Environ Microbiol. 2005;71(7):4004-13. Epub 2005/07/08. doi: 71/7/4004 [pii]10.1128/AEM.71.7.4004-4013.2005. PubMed PMID: 16000815; PubMed Central PMCID: PMC1169003.

38. Chen CY, Nace GW, Irwin PL. A 6 x 6 drop plate method for simultaneous colony counting and MPN enumeration of Campylobacter jejuni, Listeria monocytogenes, and Escherichia coli. Journal of microbiological methods. 2003;55(2):475-9. PubMed PMID: 14529971.

39. Luo Y, Sahin O, Dai L, Sippy R, Wu Z, Zhang Q. Development of a loop-mediated isothermal amplification assay for rapid, sensitive and specific detection of a Campylobacter jejuni clone. The Journal of veterinary medical science / the Japanese Society of Veterinary Science. 2012;74(5):591-6. PubMed PMID: 22188995.

40. McClure R, Balasubramanian D, Sun Y, Bobrovskyy M, Sumby P, Genco CA, et al. Computational analysis of bacterial RNA-Seq data. Nucleic Acids Res. 2013;41(14):e140. doi: 10.1093/nar/gkt444. PubMed PMID: 23716638; PubMed Central PMCID: PMC3737546.

41. Robinson JT, Thorvaldsdottir H, Winckler W, Guttman M, Lander ES, Getz G, et al. Integrative genomics viewer. Nature biotechnology. 2011;29(1):24-6. doi: 10.1038/nbt.1754. PubMed PMID: 21221095; PubMed Central PMCID: PMC3346182.

42. Thorvaldsdottir H, Robinson JT, Mesirov JP. Integrative Genomics Viewer (IGV): high-performance genomics data visualization and exploration. Briefings in bioinformatics. 2013;14(2):178-92. doi: 10.1093/bib/bbs017. PubMed PMID: 22517427; PubMed Central PMCID: PMC3603213.

43. Galperin MY, Makarova KS, Wolf YI, Koonin EV. Expanded microbial genome coverage and improved protein family annotation in the COG database. Nucleic Acids Res. 2015;43(Database issue):D261-9. doi: 10.1093/nar/gku1223. PubMed PMID: 25428365; PubMed Central PMCID: PMC4383993.

44. Hulsen T, de Vlieg J, Alkema W. BioVenn - a web application for the comparison and visualization of biological lists using area-proportional Venn diagrams. BMC Genomics.

2008;9:488. doi: 10.1186/1471-2164-9-488. PubMed PMID: 18925949; PubMed Central PMCID: PMC2584113.

45. Kanehisa M, Sato Y, Kawashima M, Furumichi M, Tanabe M. KEGG as a reference resource for gene and protein annotation. Nucleic Acids Res. 2015. doi: 10.1093/nar/gkv1070. PubMed PMID: 26476454.

46. Kery MB, Feldman M, Livny J, Tjaden B. TargetRNA2: identifying targets of small regulatory RNAs in bacteria. Nucleic Acids Res. 2014;42(Web Server issue):W124-9. doi: 10.1093/nar/gku317. PubMed PMID: 24753424.

47. Gruber AR, Lorenz R, Bernhart SH, Neubock R, Hofacker IL. The Vienna RNA websuite. Nucleic Acids Res. 2008;36(Web Server issue):W70-4. doi: 10.1093/nar/gkn188. PubMed PMID: 18424795; PubMed Central PMCID: PMC2447809.

48. Lorenz R, Bernhart SH, Honer Zu Siederdissen C, Tafer H, Flamm C, Stadler PF, et al. ViennaRNA Package 2.0. Algorithms for molecular biology : AMB. 2011;6:26. doi: 10.1186/1748-7188-6-26. PubMed PMID: 22115189; PubMed Central PMCID: PMC3319429.

49. Mou KT, Plummer PJ. The impact of the LuxS mutation on phenotypic expression of factors critical for Campylobacter jejuni colonization. Vet Microbiol. 2016;192:43-51. doi: 10.1016/j.vetmic.2016.06.011. PubMed PMID: 27527763.

50. Gallup JM, Ackermann MR. Addressing fluorogenic real-time qPCR inhibition using the novel custom Excel file system 'FocusField2-6GallupqPCRSet-upTool-001' to attain consistently high fidelity qPCR reactions. Biol Proced Online. 2006;8:87-152. doi: 10.1251/bpo122. PubMed PMID: 17033699; PubMed Central PMCID: PMCPMC1592462.

51. Surette MG, Bassler BL. Quorum sensing in Escherichia coli and Salmonella typhimurium. Proc Natl Acad Sci U S A. 1998;95(12):7046-50. PubMed PMID: 9618536; PubMed Central PMCID: PMC22733.

52. Misawa N, Blaser MJ. Detection and characterization of autoagglutination activity by Campylobacter jejuni. Infect Immun. 2000;68(11):6168-75. PubMed PMID: 11035721; PubMed Central PMCID: PMC97695.

53. Hobb RI, Fields JA, Burns CM, Thompson SA. Evaluation of procedures for outer membrane isolation from Campylobacter jejuni. Microbiology. 2009;155(Pt 3):979-88. doi: 10.1099/mic.0.024539-0. PubMed PMID: 19246768; PubMed Central PMCID: PMCPMC2763183.

54. Chang C, Xu K, Guo C, Wang J, Yan Q, Zhang J, et al. PANDA-view: an easy-to-use tool for statistical analysis and visualization of quantitative proteomics data. Bioinformatics. 2018;34(20):3594-6. doi: 10.1093/bioinformatics/bty408. PubMed PMID: 29790911; PubMed Central PMCID: PMCPMC6184437.

55. Beretta L, Santaniello A. Nearest neighbor imputation algorithms: a critical evaluation. BMC Med Inform Decis Mak. 2016;16 Suppl 3:74. doi: 10.1186/s12911-016-0318-z. PubMed PMID: 27454392; PubMed Central PMCID: PMCPMC4959387.

56. Chong J, Yamamoto M, Xia J. MetaboAnalystR 2.0: From Raw Spectra to Biological Insights. Metabolites. 2019;9(3). doi: 10.3390/metabo9030057. PubMed PMID: 30909447; PubMed Central PMCID: PMCPMC6468840.

57. Key M. A tutorial in displaying mass spectrometry-based proteomic data using heat maps. BMC bioinformatics. 2012;13 Suppl 16:S10. doi: 10.1186/1471-2105-13-S16-S10. PubMed PMID: 23176119; PubMed Central PMCID: PMCPMC3489527.

58. Croucher NJ, Thomson NR. Studying bacterial transcriptomes using RNA-seq. Curr Opin Microbiol. 2010;13(5):619-24. Epub 2010/10/05. doi: S1369-5274(10)00136-0 [pii]10.1016/j.mib.2010.09.009. PubMed PMID: 20888288; PubMed Central PMCID: PMC3025319.

59. van Vliet AH. Next generation sequencing of microbial transcriptomes: challenges and opportunities. FEMS Microbiol Lett. 2010;302(1):1-7. Epub 2009/09/09. doi: FML1767 [pii]10.1111/j.1574-6968.2009.01767.x. PubMed PMID: 19735299.

60. van Opijnen T, Camilli A. Transposon insertion sequencing: a new tool for systems-level analysis of microorganisms. Nat Rev Microbiol. 2013;11(7):435-42. doi: 10.1038/nrmicro3033. PubMed PMID: 23712350; PubMed Central PMCID: PMC3842022.

61. Butcher J, Handley RA, van Vliet AH, Stintzi A. Refined analysis of the Campylobacter jejuni iron-dependent/independent Fur- and PerR-transcriptomes. BMC Genomics. 2015;16:498. doi: 10.1186/s12864-015-1661-7. PubMed PMID: 26141822; PubMed Central PMCID: PMC4491227.

62. Chandrashekhar K, Kassem, II, Nislow C, Gangaiah D, Candelero-Rueda RA, Rajashekara G. Transcriptome analysis of Campylobacter jejuni polyphosphate kinase (ppk1 and ppk2) mutants. Virulence. 2015;6(8):814-8. doi: 10.1080/21505594.2015.1104449. PubMed PMID: 26537695.

63. Waters LS, Storz G. Regulatory RNAs in bacteria. Cell. 2009;136(4):615-28. doi: 10.1016/j.cell.2009.01.043. PubMed PMID: 19239884; PubMed Central PMCID: PMC3132550.

64. Herzberg M, Kaye IK, Peti W, Wood TK. YdgG (TqsA) controls biofilm formation in Escherichia coli K-12 through autoinducer 2 transport. J Bacteriol. 2006;188(2):587-98. doi: 10.1128/JB.188.2.587-598.2006. PubMed PMID: 16385049; PubMed Central PMCID: PMCPMC1347309.

65. Golz G, Sharbati S, Backert S, Alter T. Quorum sensing dependent phenotypes and their molecular mechanisms in Campylobacterales. Eur J Microbiol Immunol (Bp). 2012;2(1):50-60. doi: 10.1556/EuJMI.2.2012.1.8. PubMed PMID: 24611121; PubMed Central PMCID: PMCPMC3933990.

66. Xavier KB, Bassler BL. Regulation of uptake and processing of the quorum-sensing autoinducer AI-2 in Escherichia coli. J Bacteriol. 2005;187(1):238-48. doi: 10.1128/JB.187.1.238-248.2005. PubMed PMID: 15601708; PubMed Central PMCID: PMCPMC538819.

67. Holmes K, Tavender TJ, Winzer K, Wells JM, Hardie KR. AI-2 does not function as a quorum sensing molecule in Campylobacter jejuni during exponential growth in vitro. BMC Microbiol. 2009;9:214. doi: 10.1186/1471-2180-9-214. PubMed PMID: 19814796; PubMed Central PMCID: PMC2772989.

68. Adler L, Alter T, Sharbati S, Golz G. The signalling molecule Autoinducer-2 is not internalised in Campylobacter jejuni. Berl Munch Tierarztl Wochenschr. 2015;128(3-4):111-6. PubMed PMID: 25876270.

69. Plummer PJ. The mechanisms and roles of quorum sensing in the pathobiology of Campylobacter jejuni. Graduate Theses and Disseratations: Iowa State University; 2009.

70. He Y, Frye JG, Strobaugh TP, Chen CY. Analysis of AI-2/LuxS-dependent transcription in Campylobacter jejuni strain 81-176. Foodborne pathogens and disease. 2008;5(4):399-415. doi: 10.1089/fpd.2008.0106. PubMed PMID: 18713060.

71. Jeon B, Itoh K, Misawa N, Ryu S. Effects of quorum sensing on flaA transcription and autoagglutination in Campylobacter jejuni. Microbiology and immunology. 2003;47(11):833-9. PubMed PMID: 14638994.

72. Parveen N, Cornell KA. Methylthioadenosine/S-adenosylhomocysteine nucleosidase, a critical enzyme for bacterial metabolism. Mol Microbiol. 2011;79(1):7-20. doi: 10.1111/j.1365-2958.2010.07455.x. PubMed PMID: 21166890; PubMed Central PMCID: PMC3057356.

73. Mou KT. Mechanisms and roles of the LuxS system, methyl recycling, and DNA methylation on the physiology of Campylobacter jejuni. Graduate Theses and Disserations: Iowa State University; 2015.

74. Wosten MM, Wagenaar JA, van Putten JP. The FlgS/FlgR two-component signal transduction system regulates the fla regulon in Campylobacter jejuni. The Journal of biological chemistry. 2004;279(16):16214-22. doi: 10.1074/jbc.M400357200. PubMed PMID: 14960570.

75. Malik-Kale P, Parker CT, Konkel ME. Culture of Campylobacter jejuni with sodium deoxycholate induces virulence gene expression. J Bacteriol. 2008;190(7):2286-97. Epub 2008/01/29. doi: JB.01736-07 [pii]10.1128/JB.01736-07. PubMed PMID: 18223090; PubMed Central PMCID: PMC2293209.

76. Joslin SN, Hendrixson DR. Activation of the Campylobacter jejuni FlgSR two-component system is linked to the flagellar export apparatus. J Bacteriol. 2009;191(8):2656-67. doi: 10.1128/JB.01689-08. PubMed PMID: 19201799; PubMed Central PMCID: PMC2668382.

77. Hendrixson DR, DiRita VJ. Transcription of sigma54-dependent but not sigma28-dependent flagellar genes in Campylobacter jejuni is associated with formation of the flagellar secretory apparatus. Mol Microbiol. 2003;50(2):687-702. PubMed PMID: 14617189.

78. Wassenaar TM, Bleumink-Pluym NM, van der Zeijst BA. Inactivation of Campylobacter jejuni flagellin genes by homologous recombination demonstrates that flaA but not flaB is required for invasion. The EMBO journal. 1991;10(8):2055-61. PubMed PMID: 2065653; PubMed Central PMCID: PMC452888.

79. Yao R, Burr DH, Doig P, Trust TJ, Niu H, Guerry P. Isolation of motile and non-motile insertional mutants of Campylobacter jejuni: the role of motility in adherence and invasion of eukaryotic cells. Mol Microbiol. 1994;14(5):883-93. PubMed PMID: 7715450.

80. Golden NJ, Acheson DW. Identification of motility and autoagglutination Campylobacter jejuni mutants by random transposon mutagenesis. Infect Immun. 2002;70(4):1761-71. PubMed PMID: 11895937; PubMed Central PMCID: PMC127829.

81. Hendrixson DR, Akerley BJ, DiRita VJ. Transposon mutagenesis of Campylobacter jejuni identifies a bipartite energy taxis system required for motility. Mol Microbiol. 2001;40(1):214-24. PubMed PMID: 11298288.

82. Guerry P, Ewing CP, Schirm M, Lorenzo M, Kelly J, Pattarini D, et al. Changes in flagellin glycosylation affect Campylobacter autoagglutination and virulence. Mol Microbiol. 2006;60(2):299-311. doi: 10.1111/j.1365-2958.2006.05100.x. PubMed PMID: 16573682; PubMed Central PMCID: PMC1424674.

83. Logan SM, Kelly JF, Thibault P, Ewing CP, Guerry P. Structural heterogeneity of carbohydrate modifications affects serospecificity of Campylobacter flagellins. Mol Microbiol. 2002;46(2):587-97. PubMed PMID: 12406231.

84. McNally DJ, Aubry AJ, Hui JP, Khieu NH, Whitfield D, Ewing CP, et al. Targeted metabolomics analysis of Campylobacter coli VC167 reveals legionaminic acid derivatives as novel flagellar glycans. The Journal of biological chemistry. 2007;282(19):14463-75. doi: 10.1074/jbc.M611027200. PubMed PMID: 17371878.

85. Papenfort K, Vanderpool CK. Target activation by regulatory RNAs in bacteria. FEMS microbiology reviews. 2015;39(3):362-78. doi: 10.1093/femsre/fuv016. PubMed PMID: 25934124; PubMed Central PMCID: PMC4542691.

86. Merino S, Tomas JM. Gram-negative flagella glycosylation. International journal of molecular sciences. 2014;15(2):2840-57. doi: 10.3390/ijms15022840. PubMed PMID: 24557579; PubMed Central PMCID: PMC3958885.

Supporting information

S1 Appendix: Supporting Tables A through I

Table A. Plasmids used in this study.

Table B. Primers used in this study.

Table C. Summary of RNAseq results following rRNA depletion and strand specific library preparation on the Illumina HiSeq 2500 – successfully aligned reads.

Table D. Summary of RNAseq results following rRNA depletion and strand specific library preparation on the Illumina HiSeq 2500 – read mapping results.

Table E. Differential gene expression in the IA3902 ΔCjNC110 mutant as determined by RNAseq.

Table F. Differential gene expression in the IA3902 ΔluxS mutant as determined by RNAseq.

Table G. Differential gene expression in the IA3902 ΔCjNC110ΔluxS mutant as determined by RNAseq.

Table H. List of non-coding RNAs predicted by Rockhopper to exist using RNAseq transcriptomics.

Table I. Targets predicted for CjNC110 in *C. jejuni* IA3902, 137nt and 152nt predicted length, by TargetRNA2.

S2 Appendix: Suuporting Table J. List of operons in *C. jejuni* IA3902 predicted by Rockhopper to exist using RNAseq transcriptomics.

S3 Appendix: Supporting Figures A through D

Fig A. Shaking growth curve utilized for RNA extraction for RNAseq of wild-type IA3902 and isogenic mutants (mean ± SEM). A_{600} (A) and log10 CFU/mL (B) results of four replicates of a shaking growth curve performed in 250 mL Erlenmeyer flasks under microaerophilic conditions in MH broth. Analysis via two-way ANOVA revealed a statistically significant difference between strains (p <0.05), however, multiple comparison analysis of individual time points and strains when compared to wild type growth revealed that the only time point where the differences was considered to be statistically significant was at 30 hours for all strains (denoted by *).

Fig B. **COG functional categories of differentially expressed genes in the ΔCjNC110ΔluxS mutant.** Clusters of Orthologous Groups (COG) categories are indicated on the x-axis, with the number of genes enriched shown on the y-axis; blue bars indicate increased expression, red bars indicate decreased expression. C - Energy

production and conversion; D - Cell cycle control, mitosis and meiosis; E - Amino acid transport and metabolism; F - Nucleotide transport and metabolism; G - Carbohydrate transport and metabolism; H - Coenzyme transport and metabolism; I - Lipid transport and metabolism; J – Translation; K – Transcription; L - Replication, recombination and repair; M - Cell wall/membrane biogenesis; N - Cell motility; O - Posttranslational modification, protein turnover, chaperones; P - Inorganic ion transport and metabolism; Q - Secondary metabolites biosynthesis, transport and catabolism; R - General function prediction only; S - Function unknown; T - Signal transduction mechanisms; U - Intracellular trafficking and secretion; V - Defense mechanisms; W - Extracellular structures

Fig C. KEGG Pathway for flagellar assembly in *C. jejuni:* genes affected by the single mutation of either ΔCjNC110 (A) or ΔluxS (B) mutation during stationary growth phase. Blue color indicates downregulation of gene expression, red color indicates up regulation of gene expression, green indicates that the gene is present in *C. jejuni* IA3902, and white indicates that the gene is not present in IA3902.

Fig D. Graphic view of CjNC140 expression from RNAseq. (A) A screen capture from IGV of the *porA* and CjNC140 regions of the genome, corresponding to the genome structure as depicted in (B), of all of the strains sequenced using RNAseq.

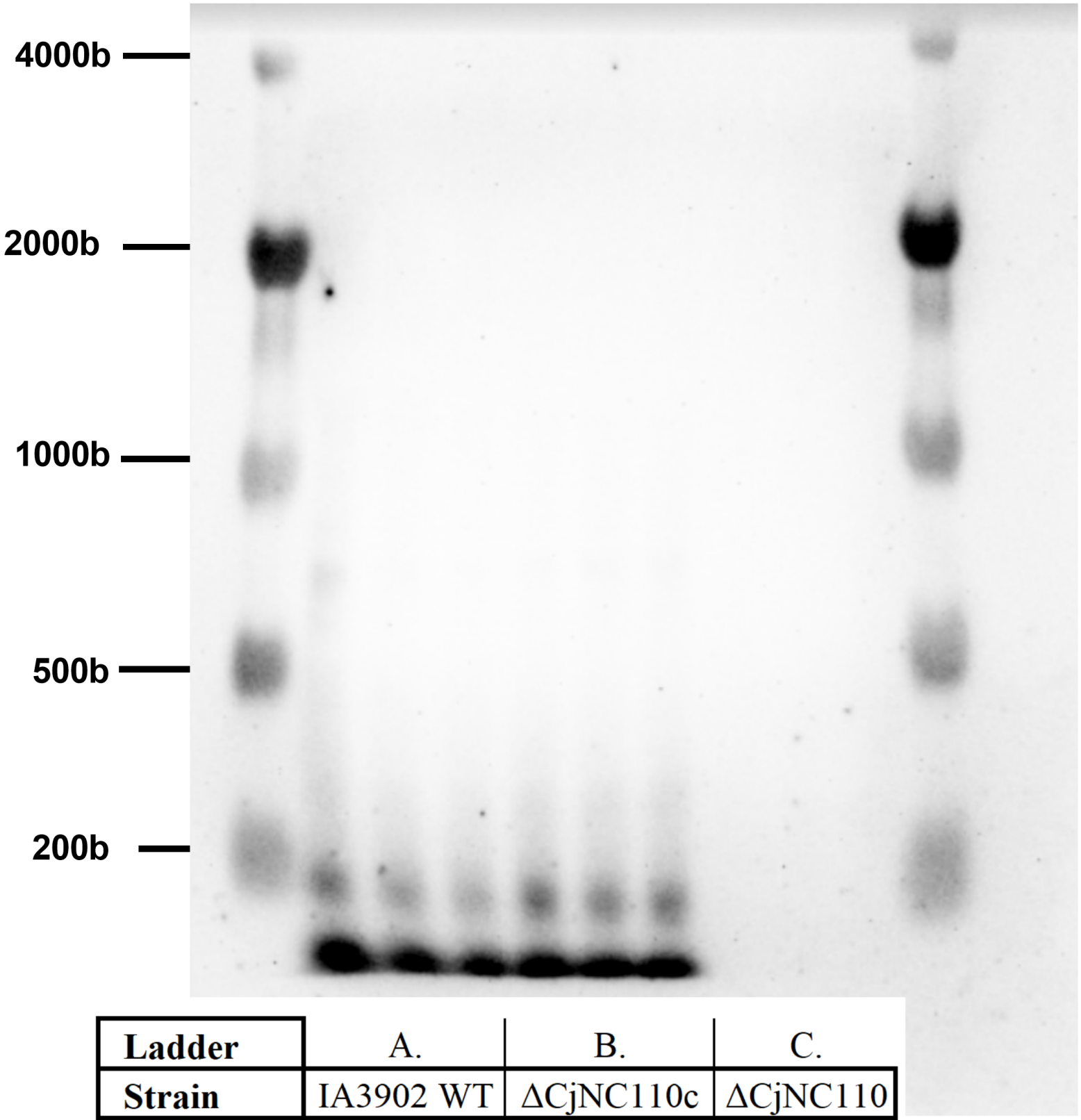

Ladder	A.	B.	C.
Strain	IA3902 WT	ΔCjNC110c	ΔCjNC110
Total RNA	15 µg/well	15 µg/well	15 µg/well

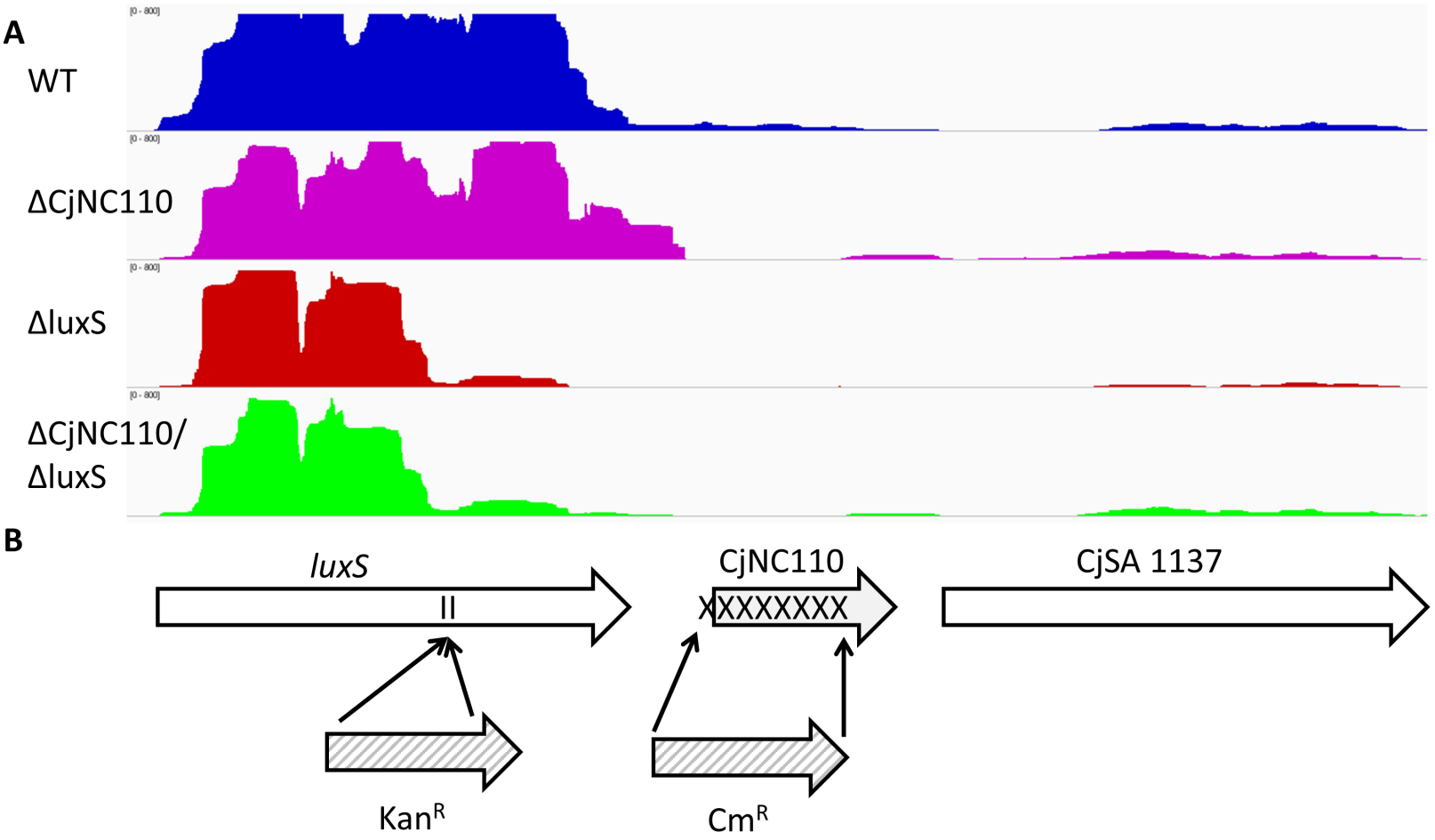
A
WT
ΔCjNC110
ΔluxS
ΔCjNC110/
ΔluxS
B
luxS
II
CjNC110
XXXXXXXX
CjSA 1137
KanR
CmR

Shared upregulated genes

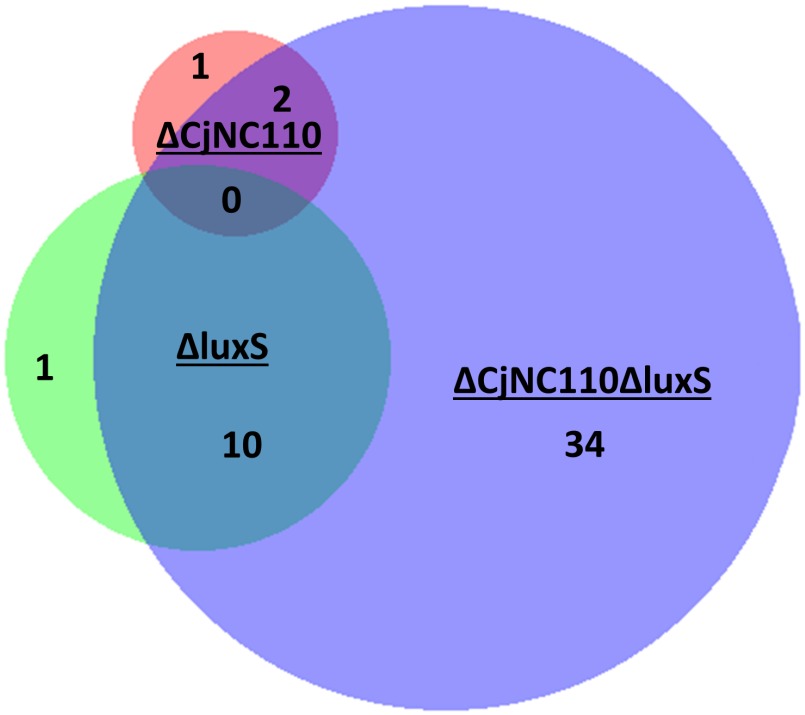

Exponential

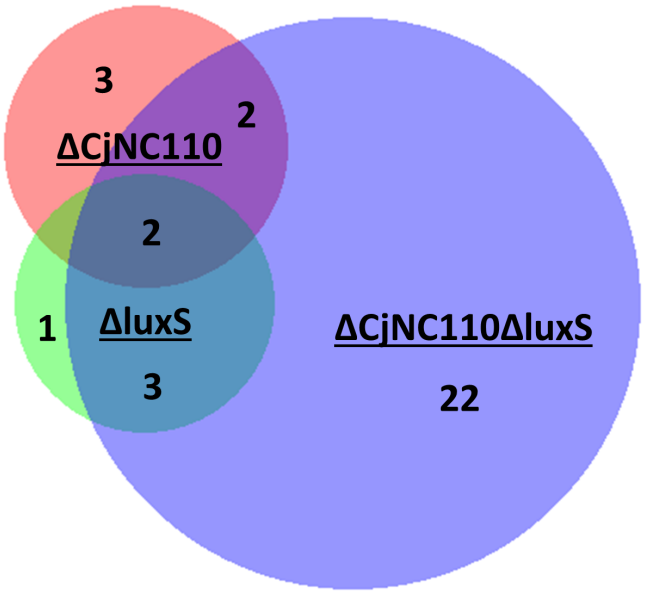

Stationary

Shared downregulated genes

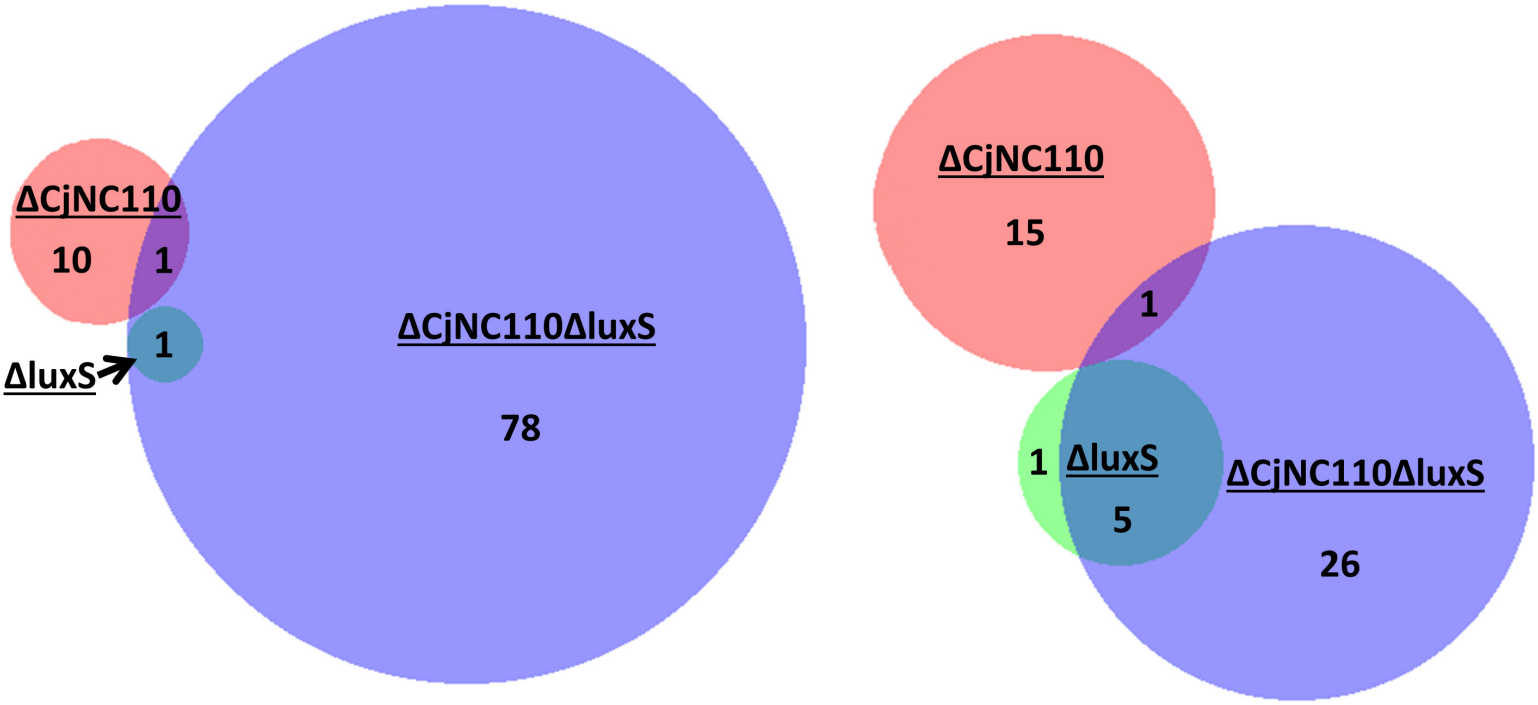

Exponential **Stationary**

Exponential

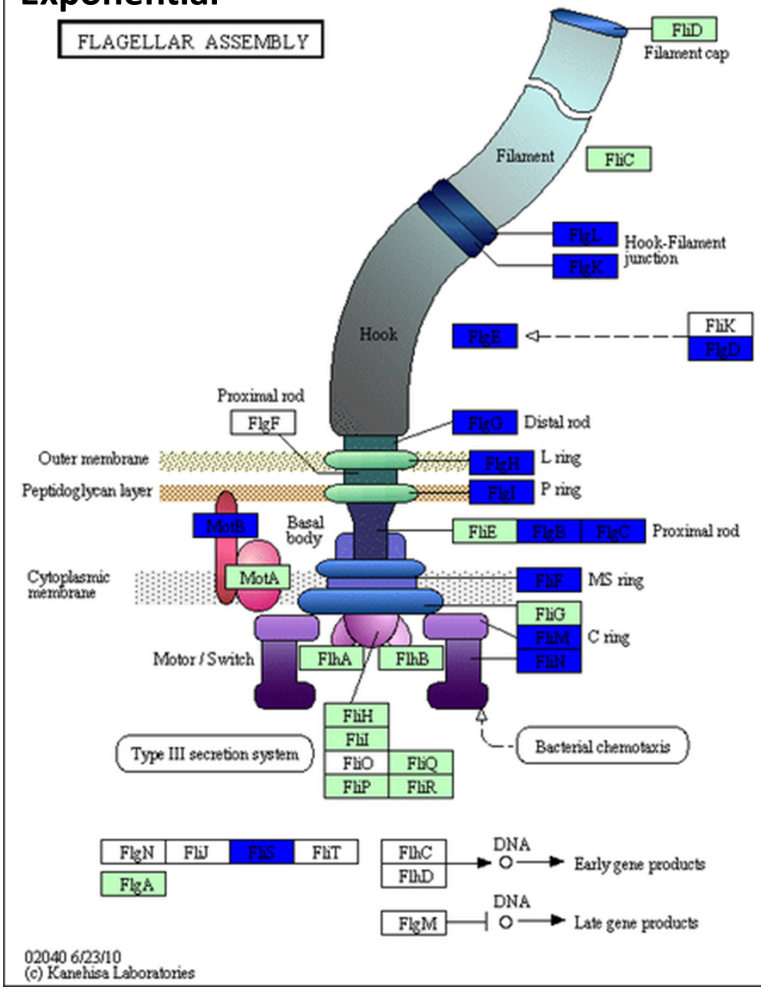

Stationary

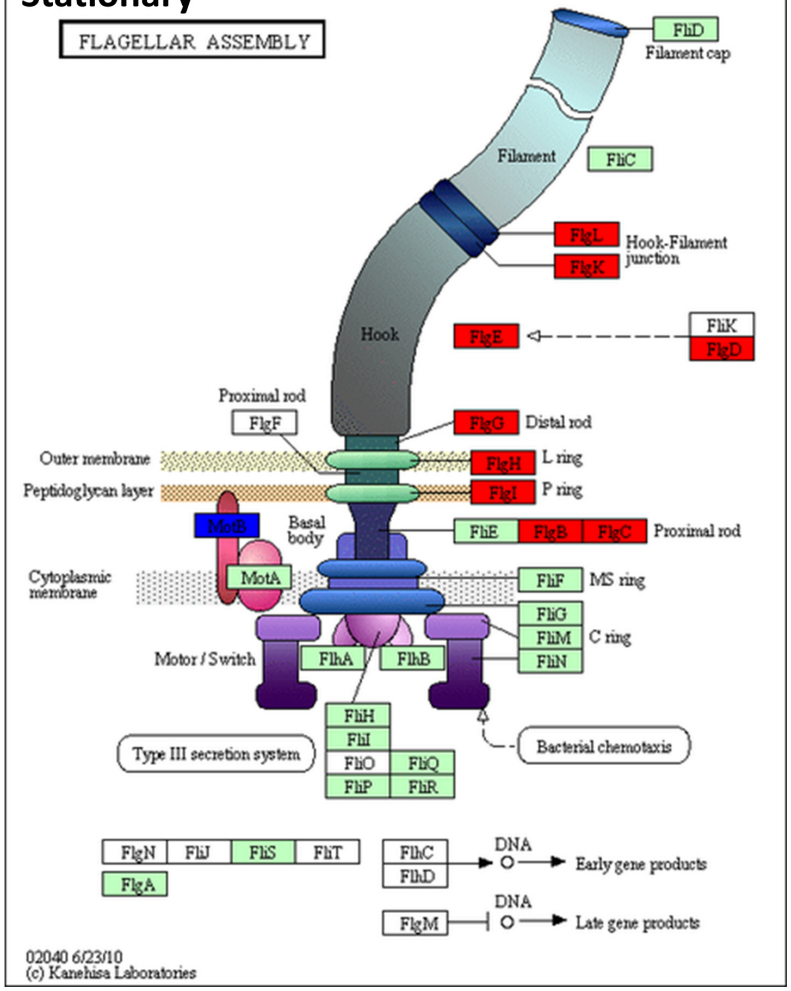

152 nt length

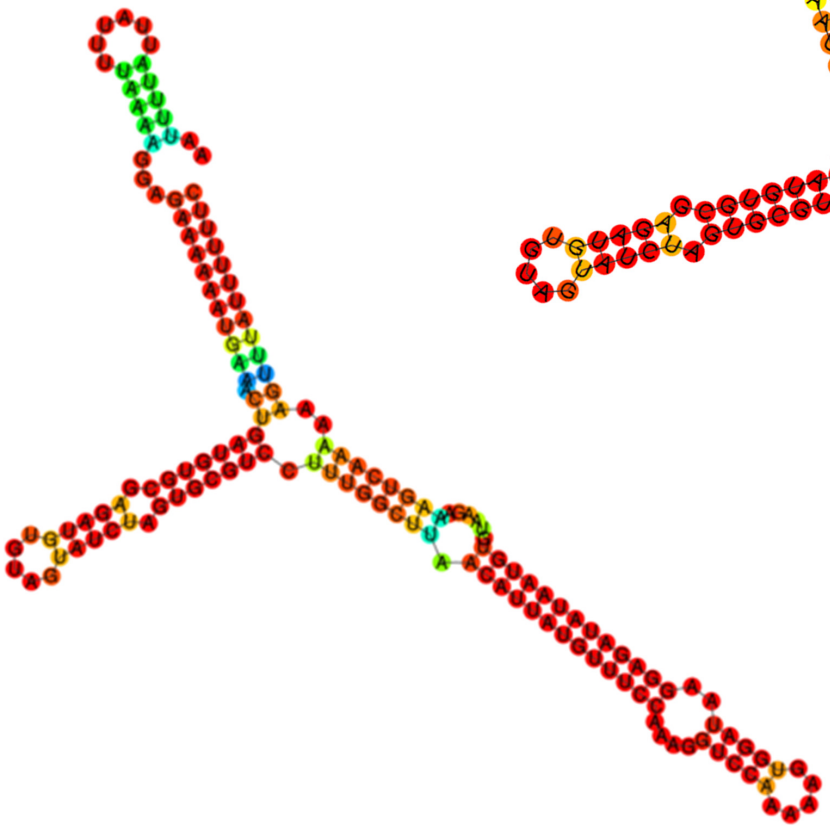

137 nt length

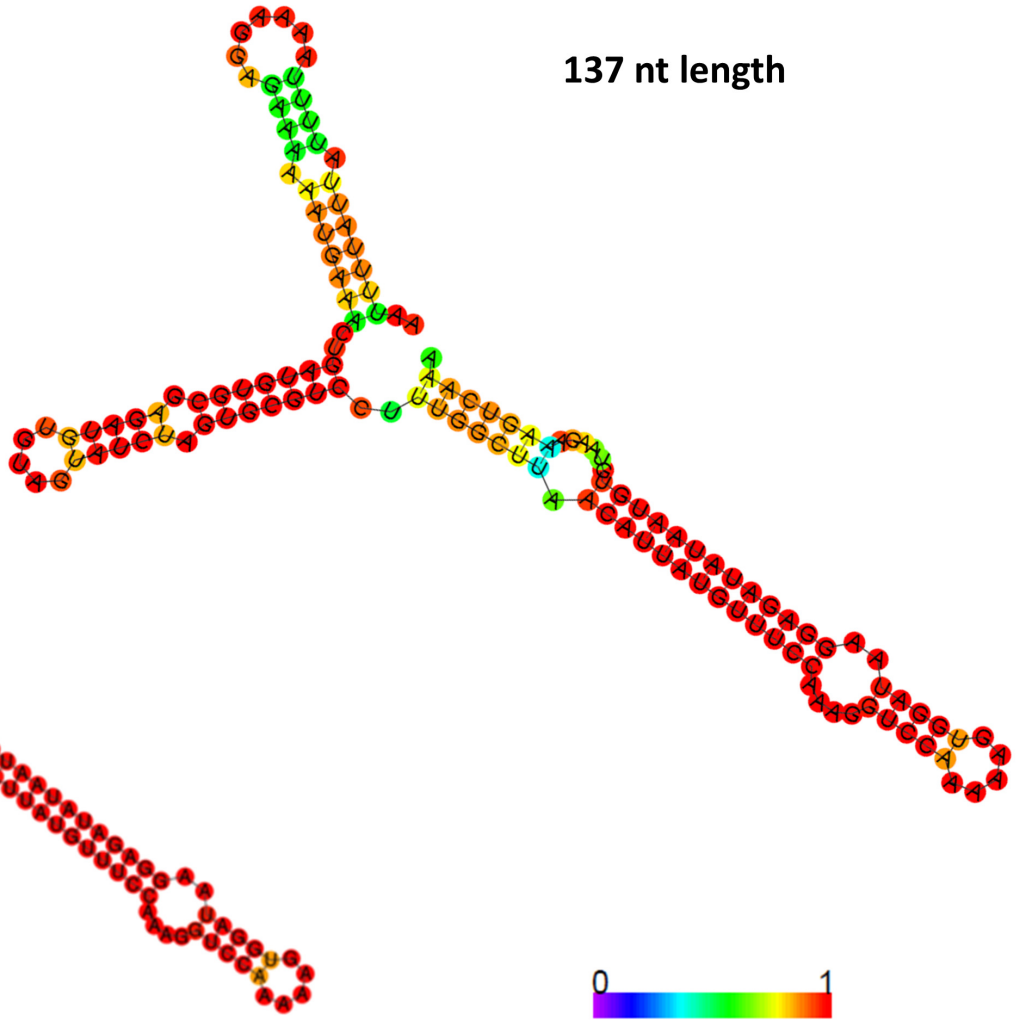

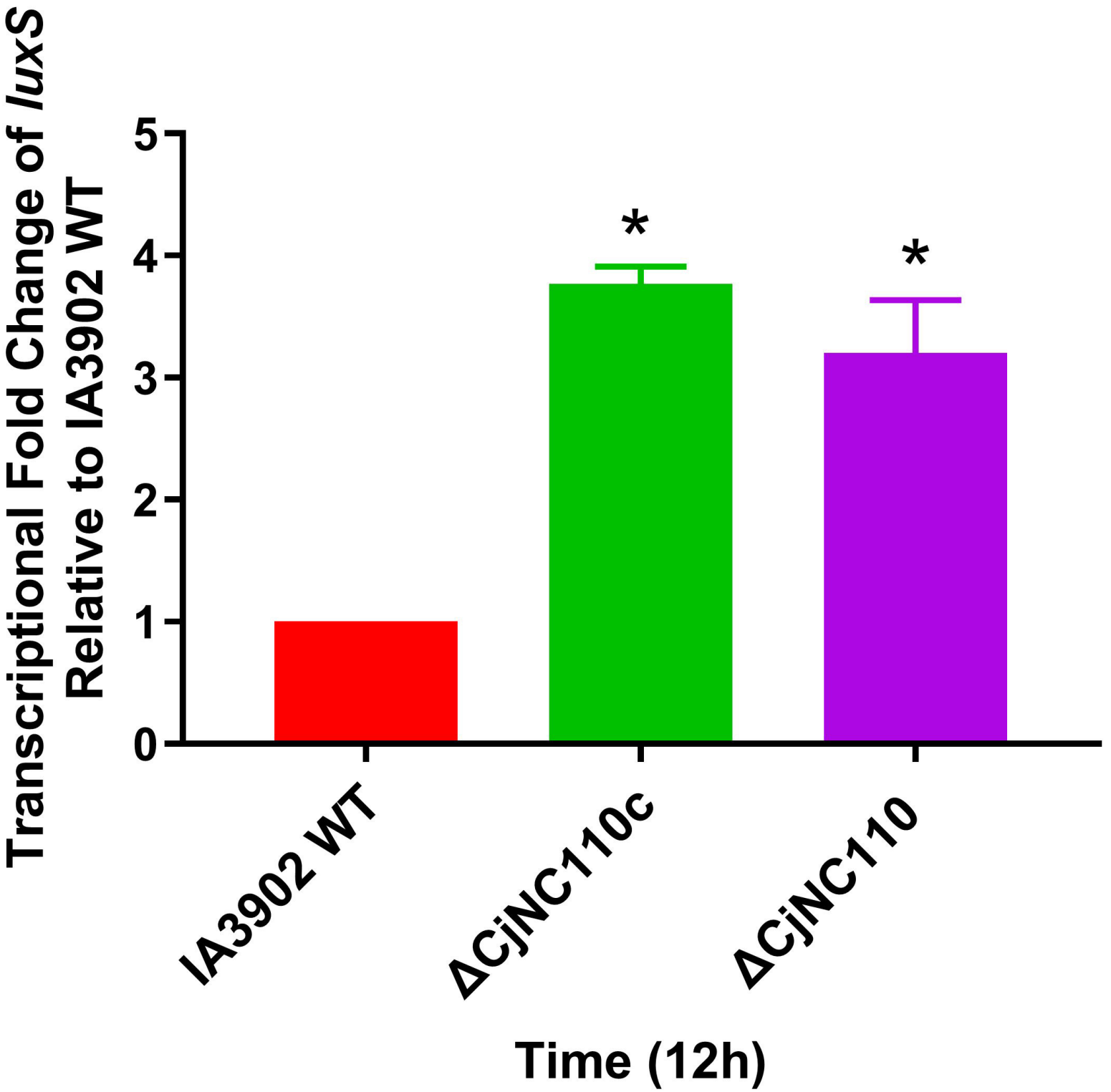
Transcriptional Fold Change of luxS
Relative to IA3902 WT
5
4
3
2
1
0
*
*
IA3902 WT
ΔCjNC110c
ΔCjNC110
Time (12h)

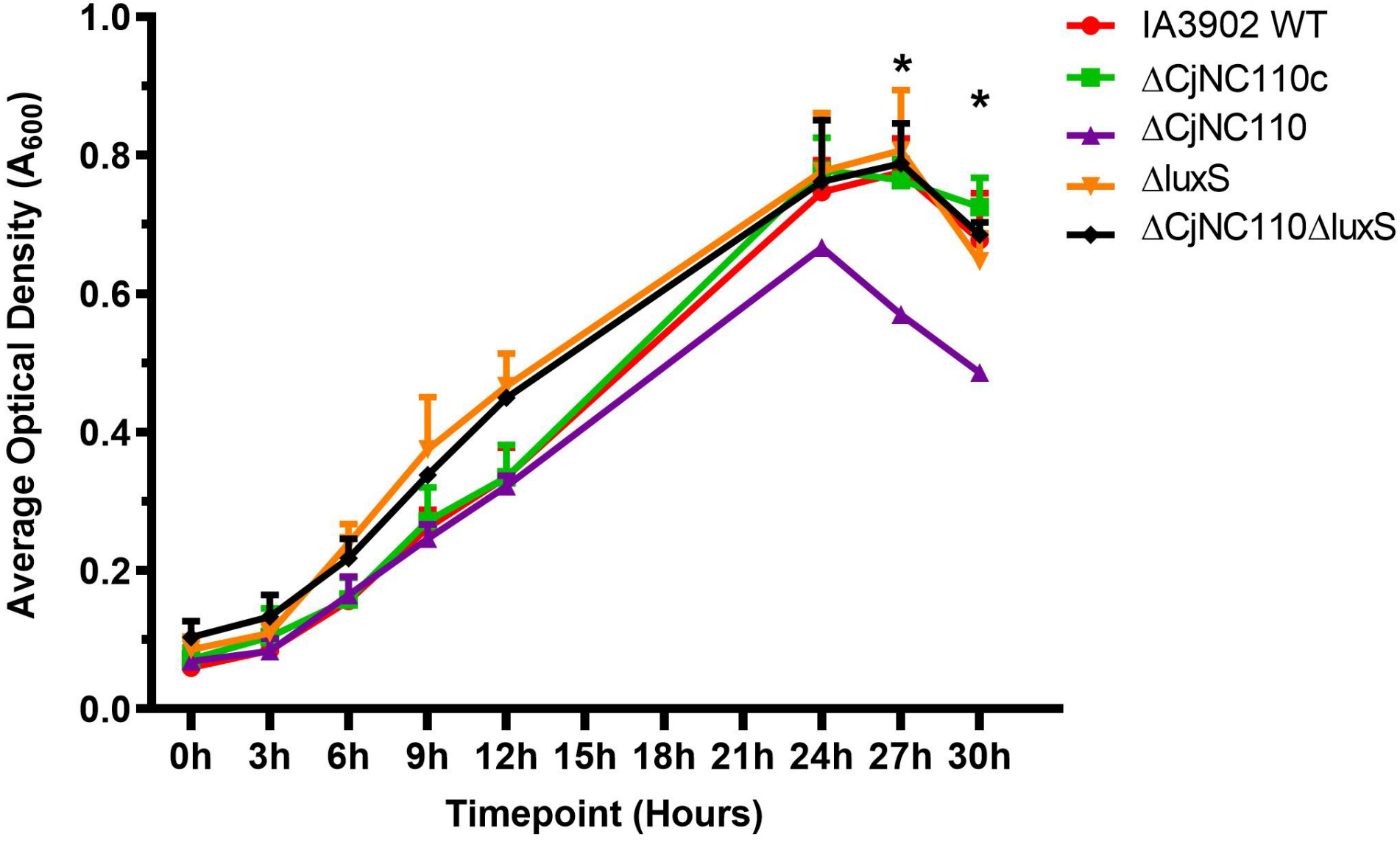
1.0
0.8
0.6
0.4
0.2
0.0
Average Optical Density (A_{600})
0h
3h
6h
9h
12h
15h
18h
21h
24h
27h
30h
Timepoint (Hours)
*
*
IA3902 WT
ΔCjNC110c
ΔCjNC110
ΔluxS
ΔCjNC110ΔluxS

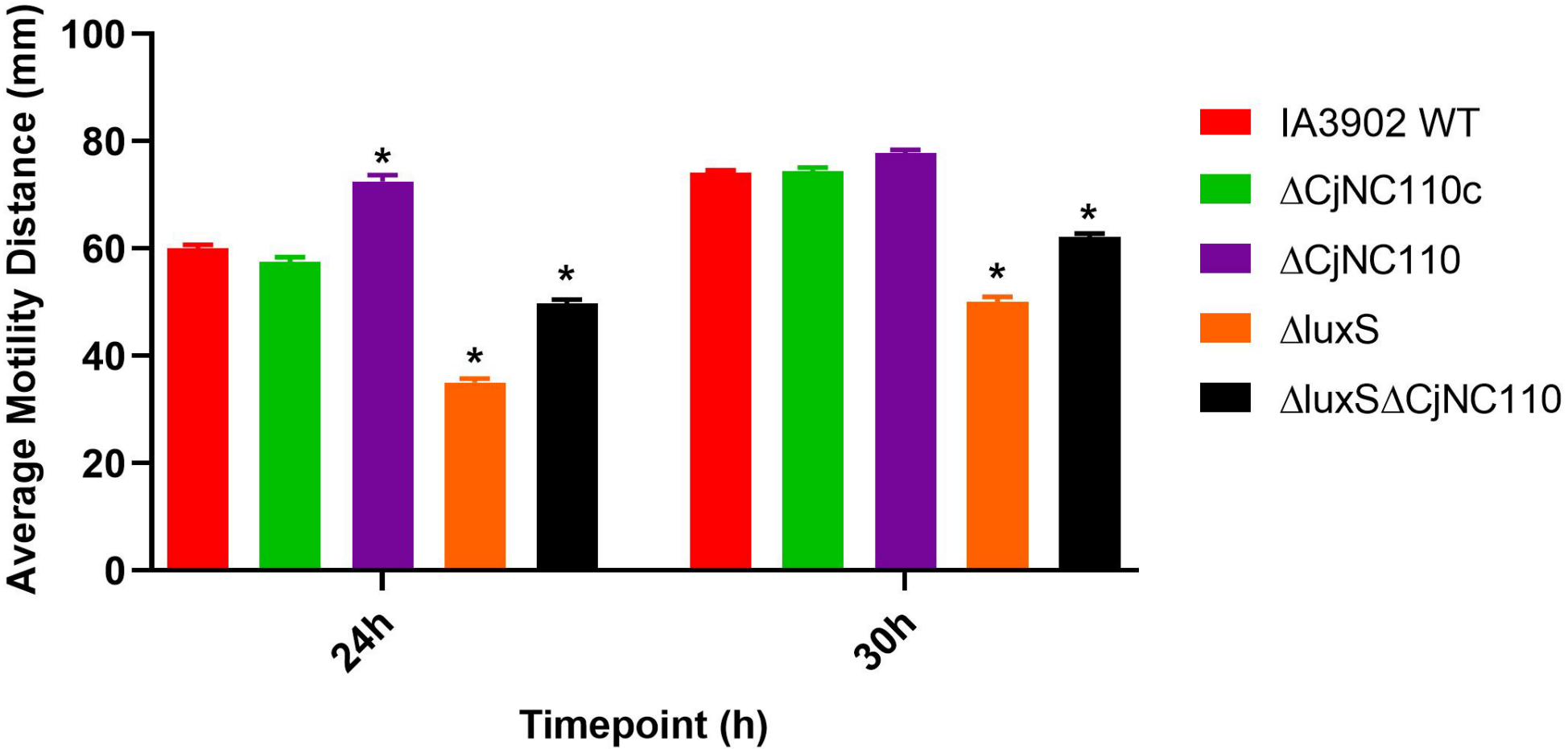
Average Motility Distance (mm)
100
80
60
40
20
0
*
*
*
*
*
24h
30h
Timepoint (h)
IA3902 WT
ΔCjNC110c
ΔCjNC110
ΔluxS
ΔluxSΔCjNC110

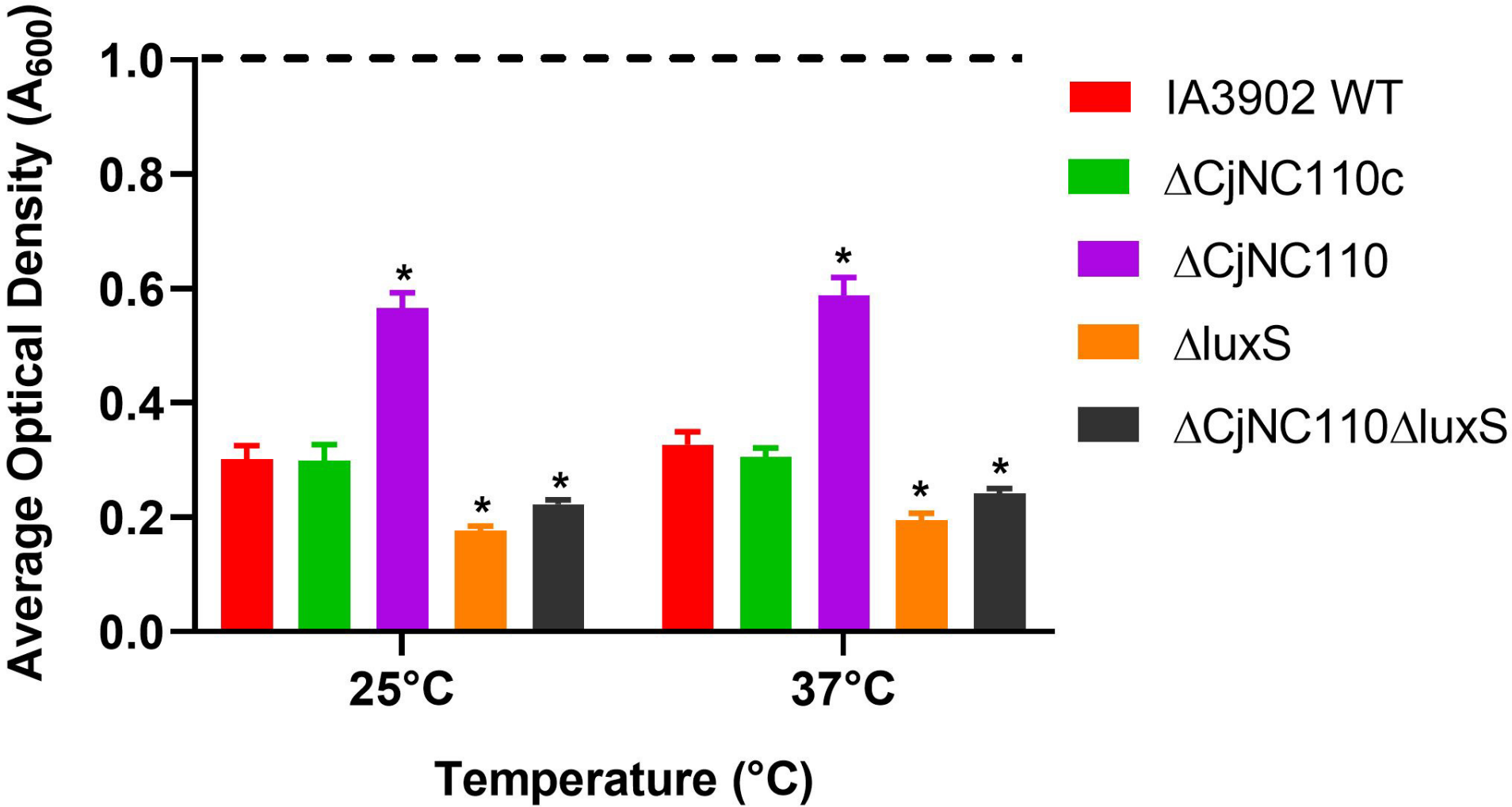
Average Optical Density (A_{600})
1.0
0.8
0.6
0.4
0.2
0.0
*
*
*
*
*
*
25°C
37°C
Temperature (°C)
IA3902 WT
ΔCjNC110c
ΔCjNC110
ΔluxS
ΔCjNC110ΔluxS

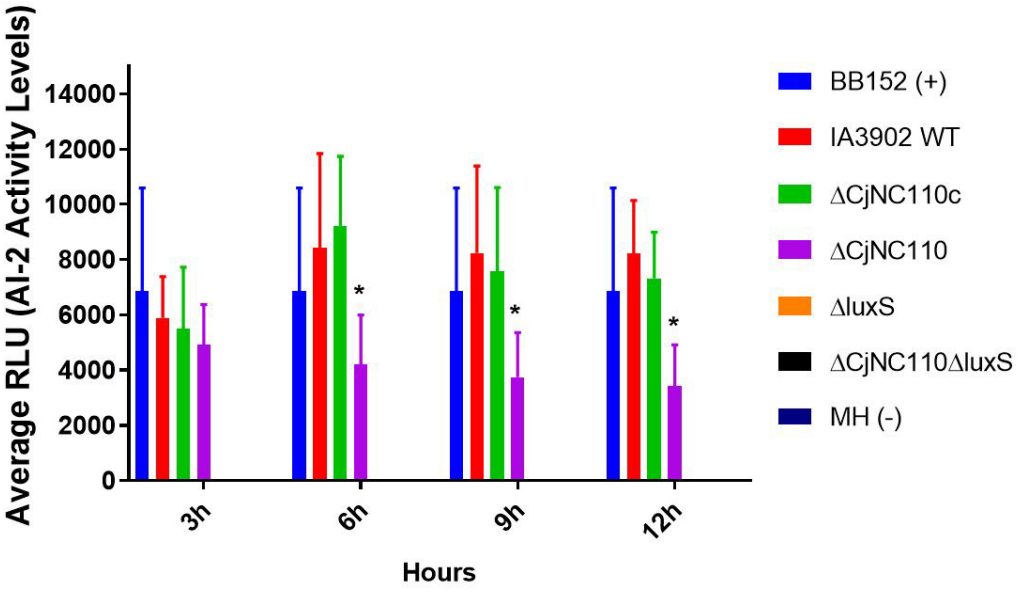
Average RLU (AI-2 Activity Levels)
14000
12000
10000
8000
6000
4000
2000
0
3h
6h
9h
12h
Hours
*
*
*
BB152 (+)
IA3902 WT
ΔCjNC110c
ΔCjNC110
ΔluxS
ΔCjNC110ΔluxS
MH (-)

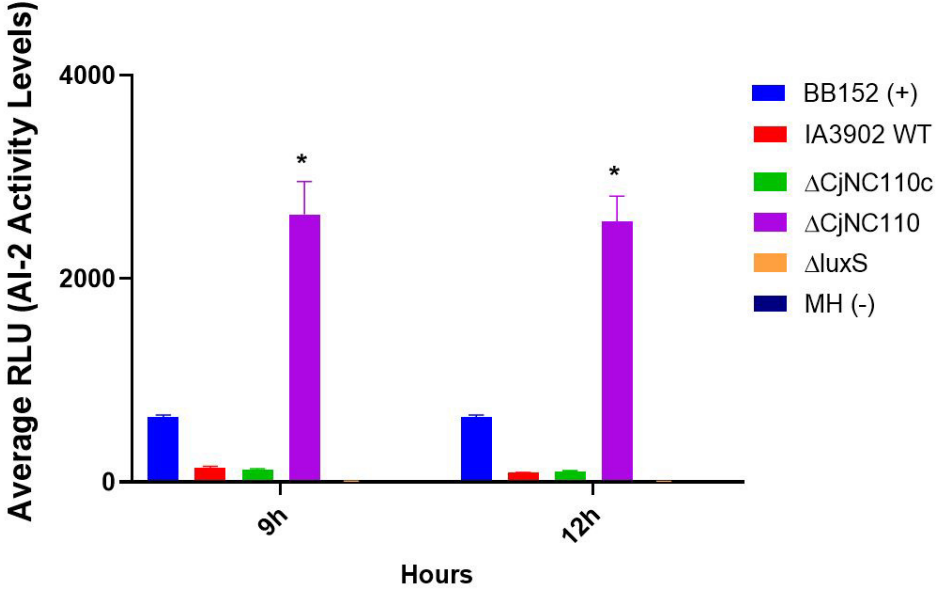
Average RLU (AI-2 Activity Levels)
4000
2000
0
9h
12h
Hours
*
*
BB152 (+)
IA3902 WT
ΔCjNC110c
ΔCjNC110
ΔluxS
MH (-)

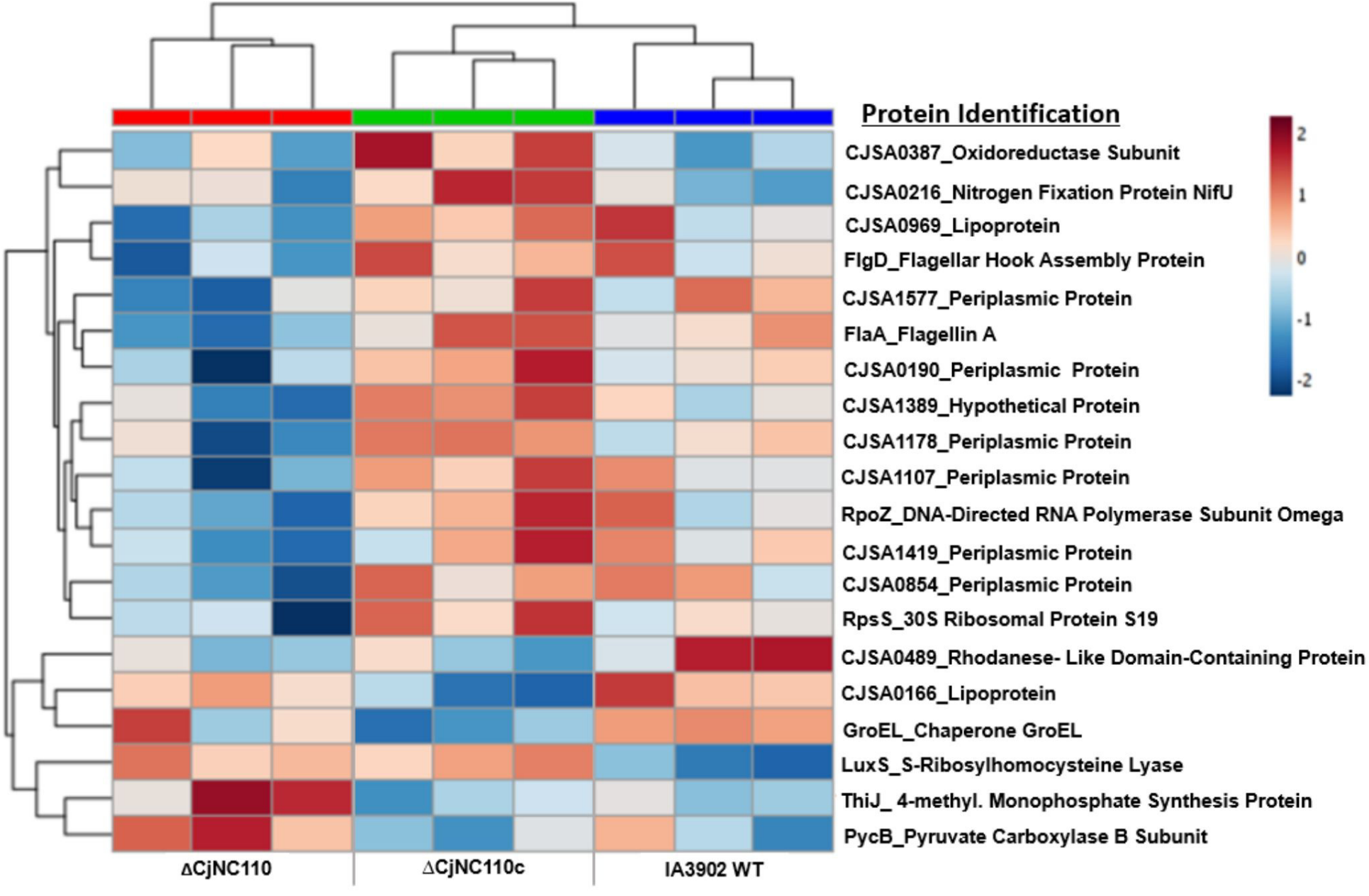
Protein Identification
CJSA0387_Oxidoreductase Subunit
CJSA0216_Nitrogen Fixation Protein NifU
CJSA0969_Lipoprotein
FlgD_Flagellar Hook Assembly Protein
CJSA1577_Periplasmic Protein
FlaA_Flagellin A
CJSA0190_Periplasmic Protein
CJSA1389_Hypothetical Protein
CJSA1178_Periplasmic Protein
CJSA1107_Periplasmic Protein
RpoZ_DNA-Directed RNA Polymerase Subunit Omega
CJSA1419_Periplasmic Protein
CJSA0854_Periplasmic Protein
RpsS_30S Ribosomal Protein S19
CJSA0489_Rhodanese- Like Domain-Containing Protein
CJSA0166_Lipoprotein
GroEL_Chaperone GroEL
LuxS_S-Ribosylhomocysteine Lyase
ThiJ_ 4-methyl. Monophosphate Synthesis Protein
PycB_Pyruvate Carboxylase B Subunit
2
1
0
-1
-2
ΔCjNC110
ΔCjNC110c
IA3902 WT

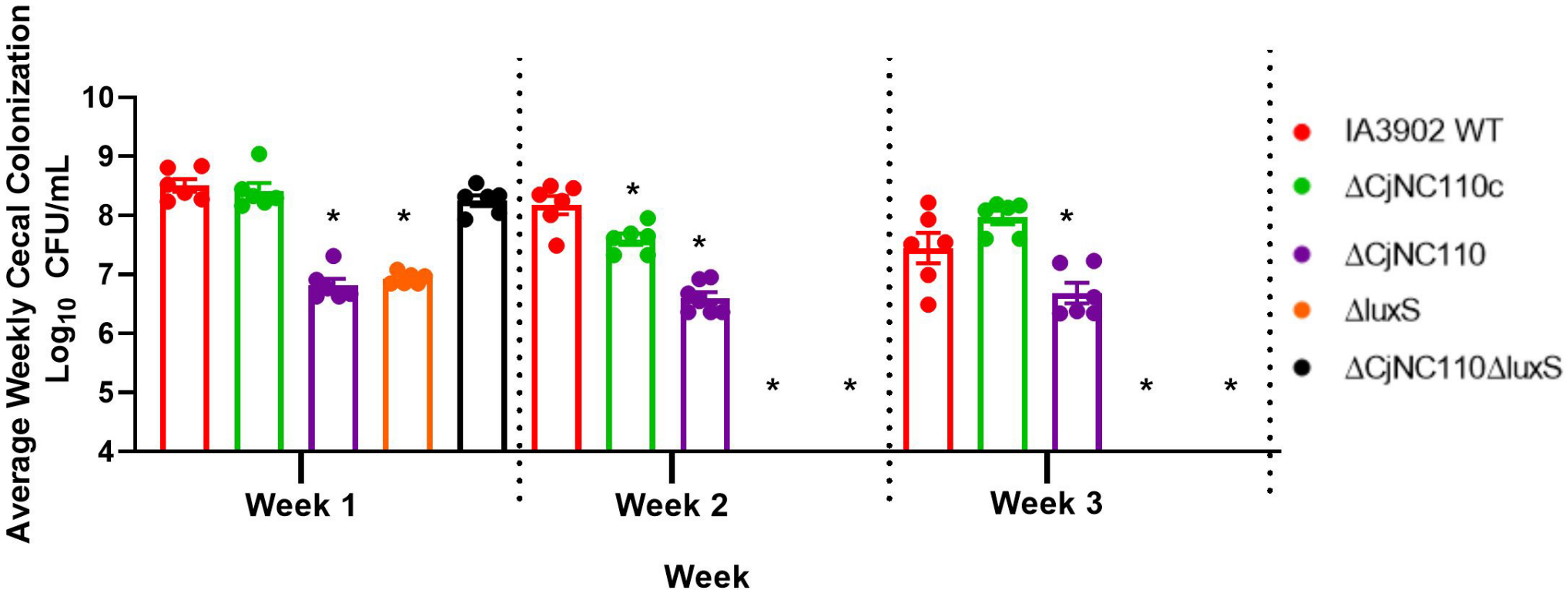
Average Weekly Cecal Colonization
Log10 CFU/mL
10
9
8
7
6
5
4
Week 1
Week 2
Week 3
Week
IA3902 WT
ΔCjNC110c
ΔCjNC110
ΔluxS
ΔCjNC110ΔluxS